Article

Cell Reports

Phase-separated nuclear bodies of nucleoporin fusions promote condensation of MLL1/CRM1 and rearrangement of 3D genome structure

Graphical abstract

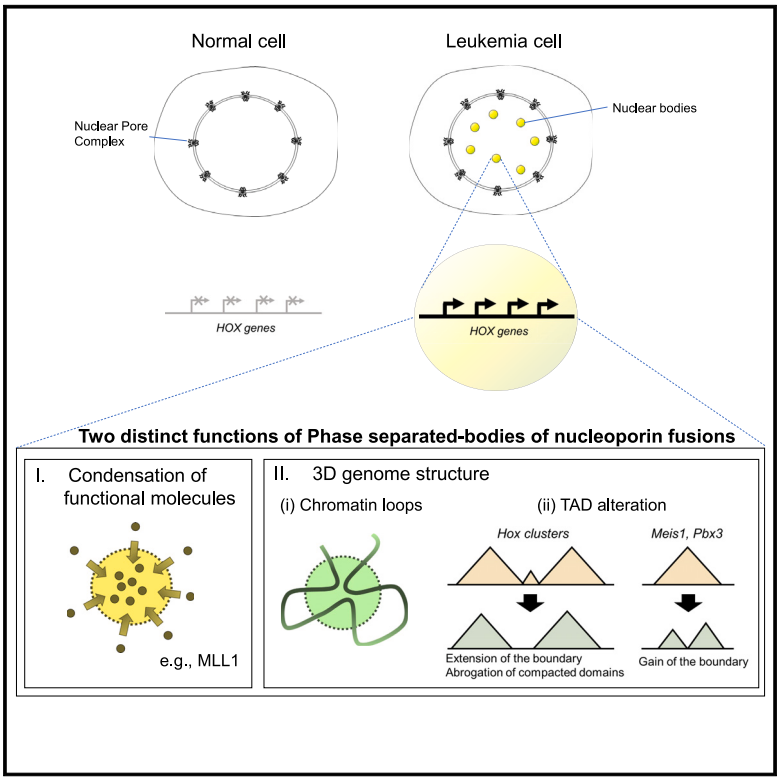

Highlights

- SET::NUP214 and NUP98:HOXA9 induce the condensation of MLL1/CRM1 at particular genomic loci
- NUP98:HOXA9 alters TAD structures and 3D genome organization
- NUP98:HOXA9 generates novel enhancers upon binding
- NUP98:HOXA9 functions by phase separation and DNA binding

Authors

Masahiro Oka, Mayumi Otani, Yoichi Miyamoto, ..., Ryuichiro Nakato, Yasuyuki Ohkawa, Yoshihiro Yoneda

Correspondence

moka@nibiohn.go.jp (M.O.), rnakato@iqb.u-tokyo.ac.jp (R.N.), yohkawa@kyushu.in (Y.O.)

In brief

Oka et al. show that nucleoporin fusion forms phase-separated bodies with two functions: condensing functional molecules (e.g., MLL1) and organizing the 3D genome structure. These functions enable target gene activation (e.g., *Hoxa* and *Hoxb* cluster genes, and *Meis1*).

Oka et al., 2023, Cell Reports *42*, 112884
August 29, 2023
https://doi.org/10.1016/j.celrep.2023.112884

CellPress

Cell Reports

CellPress
OPEN ACCESS

Article

Phase-separated nuclear bodies of nucleoporin fusions promote condensation of MLL1/CRM1 and rearrangement of 3D genome structure

Masahiro Oka,[1,2,12,*] Mayumi Otani,[1] Yoichi Miyamoto,[1] Rieko Oshima,[1] Jun Adachi,[3] Takeshi Tomonaga,[3] Munehiro Asally,[4] Yuya Nagaoka,[5] Kaori Tanaka,[6] Atsushi Toyoda,[7] Kazuki Ichikawa,[8] Shinichi Morishita,[8] Kyoichi Isono,[9] Haruhiko Koseki,[10] Ryuichiro Nakato,[5,*] Yasuyuki Ohkawa,[6,*] and Yoshihiro Yoneda[11]

[1]Laboratory of Nuclear Transport Dynamics, National Institutes of Biomedical Innovation, Health and Nutrition (NIBIOHN), 7-6-8 Saito-Asagi, Ibaraki, Osaka 567-0085, Japan

[2]Laboratory of Biomedical Innovation, Graduate School of Pharmaceutical Sciences, Osaka University, 1-3 Yamada-oka, Suita, Osaka 565-0871, Japan

[3]Laboratory of Proteomics for Drug Discovery, National Institutes of Biomedical Innovation, Health and Nutrition (NIBIOHN), 7-6-8 Saito-Asagi, Ibaraki, Osaka 567-0085, Japan

[4]School of Life Sciences, The University of Warwick, Coventry CV4 7AL, UK

[5]Institute for Quantitative Biosciences, The University of Tokyo, 1-1-1 Yayoi, Bunkyo-ku, Tokyo 113-0032, Japan

[6]Division of Transcriptomics, Medical Institute of Bioregulation, Kyushu University, 3-1-1 Maidashi, Higashi-Ku, Fukuoka 812-8582, Japan

[7]Advanced Genomics Center, National Institute of Genetics, Mishima, Shizuoka 411-8540, Japan

[8]Department of Computational Biology and Medical Sciences, Graduate School of Frontier Sciences, The University of Tokyo, 5-1-5 Kashiwanoha, Kashiwa, Chiba 277-8568, Japan

[9]Laboratory Animal Center, Wakayama Medical University, 811-1 Kimi-idera, Wakayama 641-8509, Japan

[10]Laboratory for Developmental Genetics, RIKEN Center for Integrative Medical Sciences, 1-7-29 Suehiro-cho, Tsurumi-ku, Yokohama, Kanagawa 230-0045, Japan

[11]National Institutes of Biomedical Innovation, Health and Nutrition (NIBIOHN), 7-6-8 Saito-Asagi, Ibaraki, Osaka 567-0085, Japan

[12]Lead contact

*Correspondence: moka@nibiohn.go.jp (M.O.), rnakato@iqb.u-tokyo.ac.jp (R.N.), yohkawa@kyushu.in (Y.O.)

https://doi.org/10.1016/j.celrep.2023.112884

SUMMARY

NUP98 and NUP214 form chimeric fusion proteins that assemble into phase-separated nuclear bodies containing CRM1, a nuclear export receptor. However, these nuclear bodies' function in controlling gene expression remains elusive. Here, we demonstrate that the nuclear bodies of NUP98::HOXA9 and SET::NUP214 promote the condensation of mixed lineage leukemia 1 (MLL1), a histone methyltransferase essential for the maintenance of *HOX* gene expression. These nuclear bodies are robustly associated with MLL1/CRM1 and co-localized on chromatin. Furthermore, whole-genome chromatin-conformation capture analysis reveals that NUP98::HOXA9 induces a drastic alteration in high-order genome structure at target regions concomitant with the generation of chromatin loops and/or rearrangement of topologically associating domains in a phase-separation-dependent manner. Collectively, these results show that the phase-separated nuclear bodies of nucleoporin fusion proteins can enhance the activation of target genes by promoting the condensation of MLL1/CRM1 and rearrangement of the 3D genome structure.

INTRODUCTION

NUP98 and *NUP214* are nucleoporins, components of the nuclear pore complex (NPC), and are often rearranged in leukemia.[1,2] Nucleoporin fusion genes, produced by chromosomal translocation, are associated with leukemogenesis; *NUP98* fuses with various partner genes, including homeobox transcription factors[3,4]; *NUP214* fuses with its partner genes, such as *SET* or *DEK*.[5,6]

Among the *NUP98* fusions, NUP98::HOXA9, a fusion between NUP98 and the homeobox transcription factor HOXA9,[7,8] is the best-characterized NUP98 fusion protein to date. NUP98::HOXA9 causes aberrant gene expression, which contributes to leukemogenesis.[9] Mechanistically, this fusion is associated with histone-modifying enzymes such as CREB-binding protein (CBP)/p300, HDAC1, and MLL1 (also known as KMT2A).[10–17] Additionally, NUP98 is associated with trithorax (Trx), a *Drosophila* equivalent of MLL,[18] and Wdr82-Set1A/COMPASS, another H3K4 methyltransferase.[19] SET::NUP214, a fusion of NUP214 and the histone chaperone SET,[20] interacts with MLL1 and DOT1L.[21,22] These studies suggest that the interaction between NUP-fusion proteins and histone-modifying enzymes plays an important role in triggering aberrant gene expression. Additionally, a recent study revealed that

NUP98::HOXA9 drives an aberrant three-dimensional chromatin structure that promotes malignant transformation.[23]

Intriguingly, NUP98 and NUP214 fusion proteins share three characteristics: (1) both contain dense phenylalanine-glycine (FG) repeats that are capable of forming nuclear bodies[24] through phase separation,[25] which is important for aberrant gene activation and the transformation of hematopoietic cells[23,26,27]; (2) their nuclear bodies co-localize with CRM1 (also known as XPO1),[28–33] a nuclear export receptor[34–37]; and (3) both are associated with aberrant activation of *HOX* genes, which encode the evolutionarily conserved transcription factors that function in various developmental processes.[38] *HOX* genes are dysregulated in various diseases and are particularly known to play crucial roles in leukemogenesis.[3,39–42] Taken together, these results suggest that the formation of nuclear bodies containing CRM1 is a key feature of leukemogenic NUP fusion. In support of this hypothesis, we recently discovered that CRM1 co-binds with NUP98- or NUP214-fusion proteins to chromatin at specific gene loci, including *HOX* clusters.[33,43] Moreover, CRM1 facilitates the recruitment of SQSTM1-NUP214[44] to *HOX* genes.[45]

Notably, chromatin-bound CRM1 may also play a role in other types of leukemia. It has been reported that mutant NPM1 (NPM1c), the most frequent mutation in cytogenetically normal acute myeloid leukemia, generates a novel nuclear export signal (NES) at its C terminus,[46–48] can activate *HOX* genes,[49] and also co-binds with CRM1 to the *HOX* cluster region.[43,50,51] Moreover, CALM-AF10, another NES-containing leukemogenic fusion protein, is recruited to the *HOX* cluster via CRM1.[52]

Despite this evidence, the molecular mechanism by which the formation of nuclear bodies of NUP-fusion proteins is linked to aberrant gene activation, particularly their relationship with histone-modifying enzymes, remains largely unknown.

In the present study, we investigated the potential role of NUP-fusion nuclear bodies in the activation of target genes. Our results suggest that the formation of NUP-fusion nuclear bodies is important for promoting the condensation of MLL1/CRM1 and rearrangement of the 3D genome structure at target sites to induce leukemogenic gene activation.

RESULTS

SET::NUP214 nuclear bodies co-localize with HOX-B clusters

SET::NUP214 forms CRM1-containing nuclear bodies in the human T-ALL cell line LOUCY.[30,43] To evaluate the relevance of the intranuclear localization of nuclear bodies of SET::NUP214, we performed immunolabeling combined with fluorescence *in situ* hybridization (immunoFISH). We focused on *HOX-B* clusters because our previous chromatin immunoprecipitation sequencing (ChIP-seq) data demonstrated that SET::NUP214 and CRM1 robustly accumulated at several specific loci, particularly *HOX-B* clusters, in LOUCY cells.[43] Fluorescence microscopy images of *HOX-B* clusters and SET::NUP214 nuclear bodies frequently overlapped (Figure 1A, upper panel). To quantitatively analyze this observation, we measured the shortest distance between *HOX-B* and SET::NUP214. This analysis revealed that 42.2% of the *HOX-B* clusters were localized <0.2 μm from nuclear bodies of SET::NUP214 (Figure 1B, black bars). As a negative control, we performed immunoFISH for *RNF2* loci and distance analysis (Figure 1A, lower panel; Figure 1B, red bars). Only 14.8% of *RNF2* loci were found within <0.2 μm from SET::NUP214 nuclear bodies. These results, together with our previous ChIP-seq data, strongly suggest that the nuclear bodies of SET::NUP214/CRM1 preferentially co-localize with *HOX-B* cluster regions.

SET::NUP214/CRM1 physically and functionally associated with MLL1

Next, we attempted to identify the constituents of SET::NUP214/CRM1 nuclear bodies associated with chromatin. Taking advantage of the robust accumulation of SET::NUP214/CRM1 on *HOX* clusters in LOUCY cells, we performed rapid immunoprecipitation mass spectrometry of endogenous proteins (RIME) (Figure 1C). This method uses formaldehyde to crosslink protein complexes and DNA, similar to ChIP-seq, and has been used to identify chromatin-bound proteins associated with target molecules.[53] Our RIME data demonstrated that NUP214 and CRM1 were strongly bound to each other or existed in the same complex, as their signals were primarily observed in both anti-NUP214 and anti-CRM1 immunoprecipitates (IPs) (Table S1). We first confirmed that SET was present in anti-NUP214 IPs, demonstrating successful immunoprecipitation of the SET::NUP214 fusion. To identify the factors that are involved in the function of SET::NUP214/CRM1 nuclear bodies, we then focused on the proteins that are abundant both in anti-NUP214 IPs and anti-CRM1 IPs, but not in control IPs (strict criteria were used to select the candidate proteins whose peptide counts are either "0" or "1" in the control IP). We also found the majority of nucleoporins (22 nucleoporins) together with nuclear transport receptors or RAN and its regulators in both IPs (Figure 1D and Table S1). We omitted the nucleoporins or proteins involved in nuclear transport from our analysis because they are likely associated with endogenous NUP214 or CRM1 in NPCs. Interestingly, the analysis revealed several proteins whose relationship with NPC or nuclear transport is not known to date, but are strongly associated with both NUP214 and CRM1, namely ADAR, MLL1, striatin, and TRAF3IP (T3JAM) (Figure 1D). We also identified MX2, an antiviral protein that interacts with several nucleoporins.[54]

To further analyze these five proteins, knockdown of the five candidate genes was performed in LOUCY cells to monitor their effect on the expression of *HOX* genes, which are dependent on SET::NUP214. The fold change in *HOX* gene expression was measured in LOUCY cells using qPCR (Figure 1E). We found that the knockdown of MLL1 substantially decreased the expression of *HOX* genes (Figures 1E and S1). We also found that the knockdown of striatin, a scaffold protein involved in the regulation of signaling pathways,[55] decreased the expression of *HOX* genes. Knockdown of other candidate genes did not affect *HOX* expression. Because the effect of MLL1 knockdown was more evident than that of the other knockdowns, we focused our analysis on MLL1.

To characterize MLL1, LOUCY cells were co-stained with anti-CRM1 and anti-MLL1 or anti-NUP214 antibodies (Figure 2A,

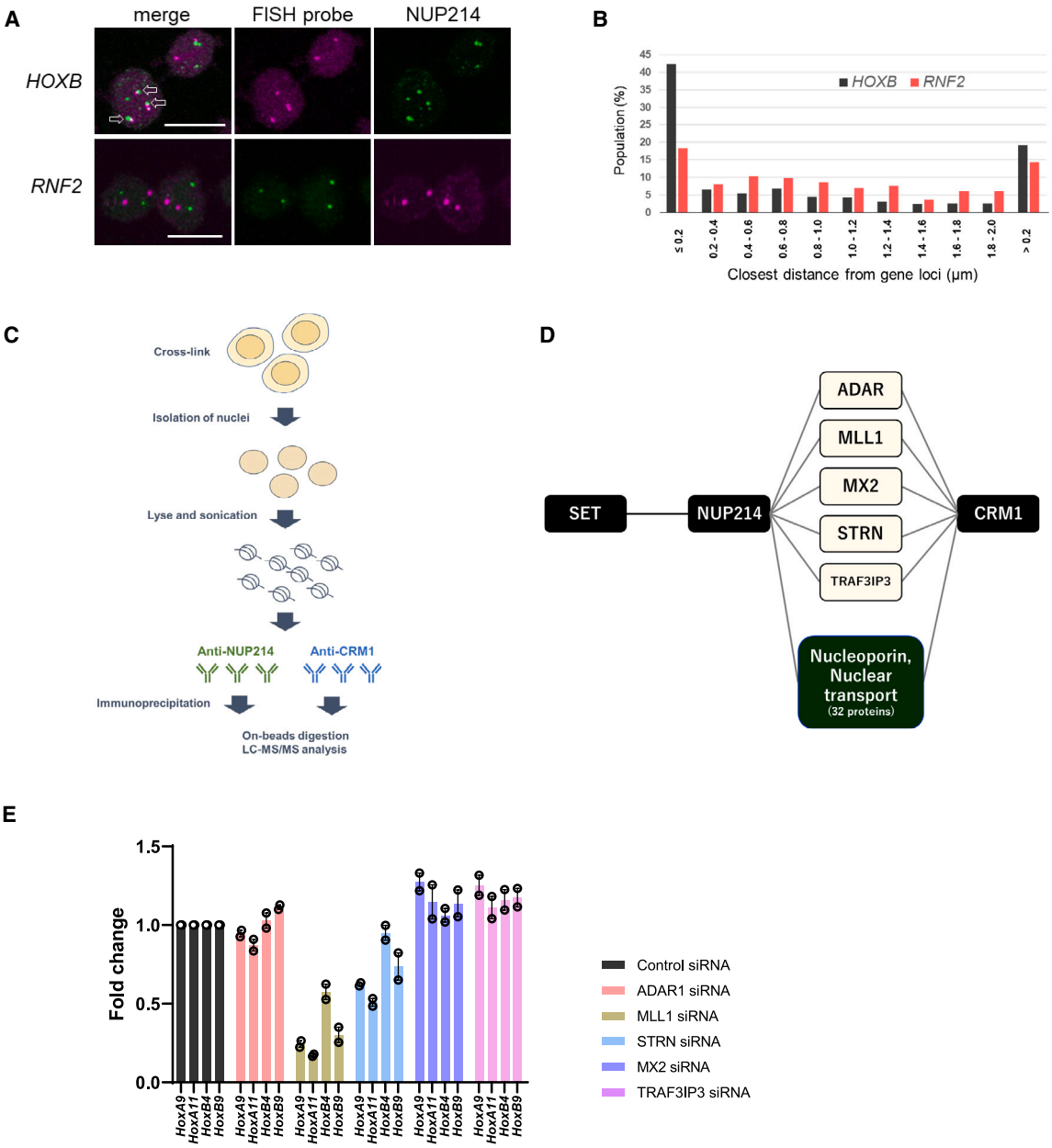

Figure 1. SET::NUP214 and CRM1 physically and functionally associate with MLL1

(A and B) Subcellular localization of SET::NUP214 and *HOX-B* or *RNF2* (control) gene loci in LOUCY cells. (A) ImmunoFISH was performed to detect SET::NUP214 nuclear bodies and respective gene loci. *HOX-B* cluster region is frequently found adjacent to SET::NUP214 nuclear bodies (open arrows) compared with *RNF2*. Scale bars, 10 μm. (B) The minimum distance between each gene locus (as revealed by FISH) and the closest SET::NUP214 nuclear bodies were analyzed using ImageJ (n = 531 for *HOX-B*, n = 397 for *RNF2*).

(C) Schematic of RIME used in this study.

(D) Schematic summary of the RIME results.

(E) Effect of knockdown of candidate components of SET::NUP214 nuclear bodies. Knockdown of ADAR1, KMT2A, STRN, MX2, and TARFIP3 was performed by nucleofection of small interfering RNA (siRNA) in LOUCY cells. The effect of knockdown on *HOX* gene expression (*HOXA9*, *HOXA11*, *HOXB4*, and *HOXB9*) was examined 4 days after nucleofection. *GAPDH* was used as the reference gene. Data are mean of two independent experiments.

upper two rows). MLL1 frequently co-localized with SET::NUP214/CRM1 nuclear bodies in LOUCY cells, which is consistent with a recent report.[22] To examine whether the partner proteins of MLL1 also co-localize with nuclear bodies, we immunostained menin, which has been shown to interact with MLL1 physically and functionally.[56,57] Immunostaining revealed that menin also co-localized with SET::NUP214/CRM1 nuclear bodies (Figure 2A, bottom row).

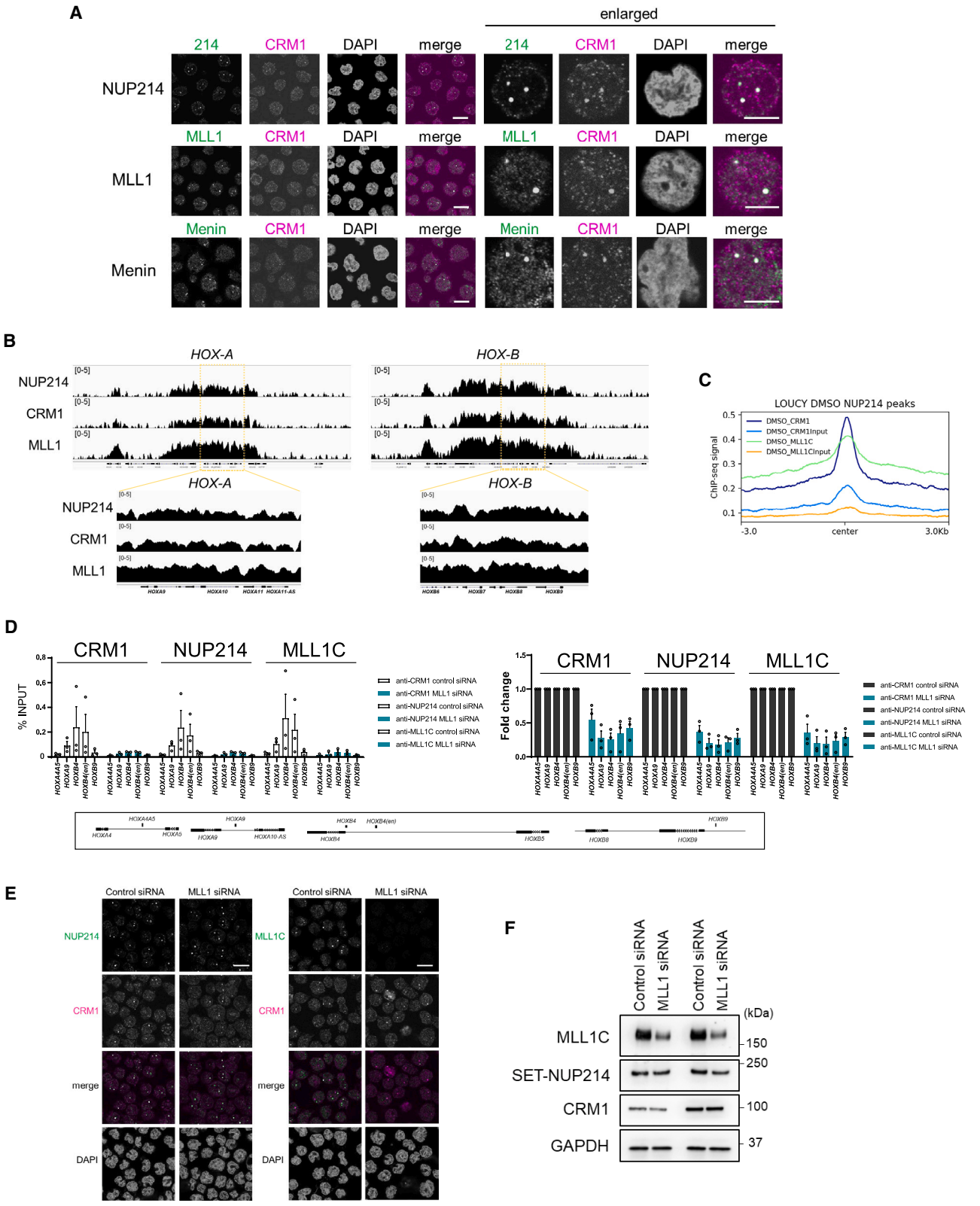

(legend on next page)

SET::NUP214/CRM1/MLL1 show genome-wide co-localization and are essential constituents of the nuclear bodies

To characterize the relevance of the association between MLL1, SET::NUP214, and CRM1 in genome-wide binding, we performed ChIP-seq analyses. Strikingly, the binding sites of these proteins showed frequent co-occupancy on a genome-wide scale, including *HOX-A* and *HOX-B* cluster regions and other SET::NUP214 binding sites, such as *CDKN2C* (Figures 2B, 2C, and S2A). However, we did not find any obvious genome-wide association between these proteins and the transcription start site (TSS), gene body, or enhancer (Figure S2B). These results suggest that NUP214, CRM1, and MLL1 accumulate in several distinct regions without any obvious genome-wide binding patterns.

Next, we examined the role of MLL1 in SET::NUP214/CRM1 accumulation in *HOX* clusters. ChIP-qPCR analysis revealed that MLL1 knockdown caused a significant decrease in SET::NUP214 and CRM1 signals in *HOX* clusters (Figure 2D), *CDKN2C*, *CLEB2B*, and *COMMD3-BMI* (Figure S2C). In *HOX* clusters, the effects of MLL1 knockdown were more pronounced than in other regions. We also found that neither the formation of SET::NUP214/CRM1 nuclear bodies nor the protein expression of CRM1 and SET::NUP214 was affected by the knockdown of MLL1 (Figures 2E and 2F). Therefore, MLL1 most likely plays a role in the recruitment of NUP214/CRM1 bodies to target loci rather than in the assembly of nuclear bodies.

We then examined the effect of the CRM1 inhibitor KPT-330, which covalently binds to CRM1 to inhibit its export activity and induce its degradation[58] and disassembly of SET::NUP214 nuclear bodies.[43] We found that SET::NUP214 nuclear bodies were diminished when incubated with 100 nM KPT-330 for 24 h and were almost completely disrupted at 1,000 nM (Figure S2D), consistent with our previous study.[43] Furthermore, ChIP-qPCR revealed a dose-dependent effect of KPT-330 on the chromatin binding of SET::NUP214/CRM1/MLL1 (Figure S2E). Importantly, even though treatment with 1,000 nM KPT-330 showed some degree of cytotoxic effect concomitant with apoptotic cell death, we detected no sign of cytotoxicity/apoptosis at 100 nM KPT-330 (Figures S2F and S2G), the concentration at which SET::NUP214 inhibition was observed.

Next, we examined the effect of KPT-330 on MLL1 protein levels, as we previously showed that it affects the stability of SET::NUP214.[43] We included leptomycin B (LMB),[59] another CRM1 inhibitor that disassembles SET::NUP214 nuclear bodies[29,30] and destabilizes the SET::NUP214 protein[43] without inducing the degradation of CRM1, which contrasts with KPT-330. Our findings revealed that neither KPT-330 nor LMB significantly affected the levels of MLL1 protein (Figure S2H), although LMB showed a greater cytotoxic effect than 1,000 nM KPT-330 (Figure S2F). These results demonstrated that CRM1 is critical for the stable assembly of SET::NUP214 nuclear bodies associated with MLL1 on chromatin.

Collectively, our results suggest that the binding of SET::NUP214 to *HOX* cluster regions is maintained by MLL1 and CRM1, indicating that SET::NUP214/CRM1/MLL1 forms functional nuclear bodies that associate with *HOX* cluster regions to robustly activate *HOX* genes.

Phase separation and DNA binding of NUP98::HOXA9 are important for its targeting and downstream gene activation

Previous studies have reported unexpected similarities between the nuclear bodies formed by SET::NUP214 and NUP98::HOXA9; namely, both accumulate in *HOX* cluster regions[15,21,33,43] and contain CRM1.[28,31–33] NUP98::HOXA9 is physically and functionally associated with MLL1 in the hematopoietic progenitor cells.[14,15] However, the relevance of the nuclear bodies of NUP98::HOXA9 to MLL1 remains unknown. These results prompted us to investigate the relationship between MLL1 and nuclear bodies formed by NUP98::HOXA9.

To investigate the function of NUP98::HOXA9, we isolated mouse embryonic stem cells (mESCs) stably expressing FLAG-tagged NUP98::HOXA9 because we demonstrated that *Hox* genes are selectively activated in these cells.[33] First, we performed immunoFISH to monitor the co-localization of *Hox* loci and FLAG-NUP98::HOXA9. Our data revealed that the nuclear bodies of NUP98::HOXA9 frequently co-localized with *Hoxa* loci as compared with negative control loci (outside *Cdkn2a*) (36.7% or 18.2% localized <0.2 μm from the nuclear bodies, respectively) (Figures 3A and 3B).

Next, to determine the importance of chromatin-associated nuclear bodies formed by NUP98::HOXA9, we established cell lines carrying mutated NUP98::HOXA9 (Figure 3C). The AG mutant (mutated from FG to AG; a total of 38 FG) is deficient in phase separation, and the N51S mutant (possessing a point mutation in the homeodomain [N51S][60]) is deficient in binding DNA. In addition, we generated a GAFG mutant (mutated from GLFG to GAFG; a total of nine GLFGs), which has also been reported to affect phase-separating ability.[61] Introducing the AG mutation completely abolished nuclear body formation (Figure 3D). As for the GAFG mutation, although we still observed some nuclear

Figure 2. MLL1 is an essential component of SET::NUP214 nuclear bodies to recruit and activate target genes

(A) SET::NUP214 nuclear bodies co-localized with CRM1, MLL1, and menin. LOUCY cells were immunostained with anti-NUP214, MLL1C, menin, and CRM1 antibodies. The merged images of CRM1 are shown. Nuclei were stained with DAPI. Scale bars, 10 μm (5 μm for enlarged images).

(B) Binding profiles of NUP214, CRM1, and MLL1C in LOUCY cells at *HOX-A* and *HOX-B* cluster regions. A more detailed view is shown at the bottom of each.

(C) Aggregation plots of CRM1 and MLL1C binding sites in LOUCY. CRM1 and MLL1C binding signals are mapped against NUP214 binding sites.

(D) (Left) ChIP-qPCR analysis of CRM1, NUP214, and MLL1 at *HOX* gene loci in LOUCY cells treated either with control siRNA or MLL1 siRNA for 4 days. (Right) ChIP-qPCR data were analyzed for the ratio as compared with control siRNA. The primer set used was as follows: *HOXA4A5* (intergenic region between *HOXA4* and *HOXA5*); *HOXA9* (promoter); *HOXB4* (promoter); *HOXB4* (enhancer); *HOXB9* (promoter). Their binding sites are indicated in the boxed area (bottom). Data are presented as mean values ± SEM of three independent experiments (n = 3).

(E) siRNA (control or MLL1) treated LOUCY cells were immunostained with indicated antibodies. The merged images of CRM1 are shown. Nuclei were stained with DAPI. Scale bar, 10 μm.

(F) Immunoblotting was performed to monitor the effect of siRNA treatment (control or MLL1) on indicated proteins.

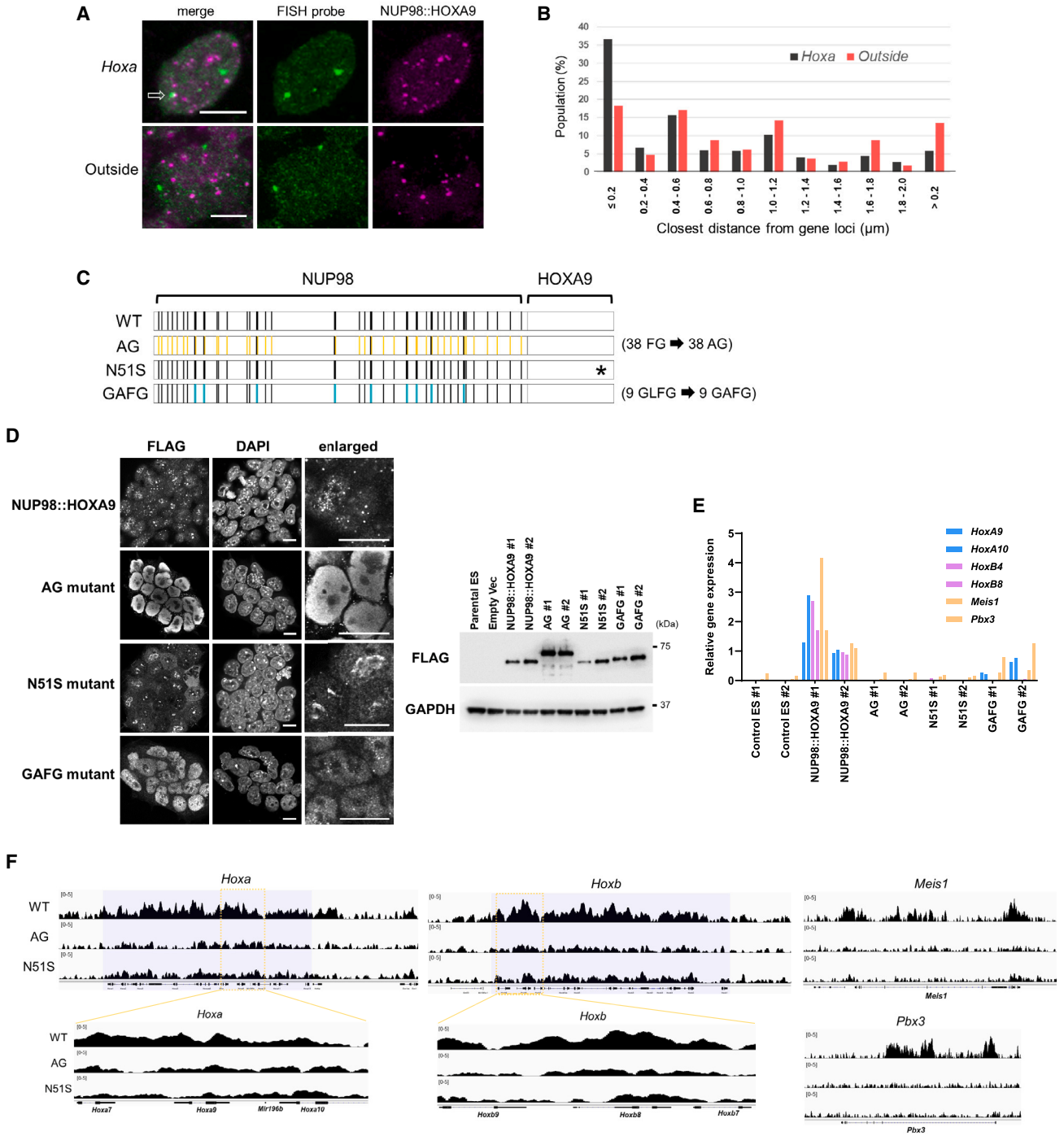

Figure 3. FG repeat and homeodomain of NUP98::HOXA9 are important for its accumulation on *HOX* clusters and gene activation

(A and B) Subcellular localization of NUP98:HOXA9 and *Hoxa* or Outside (control: ~200 kb distant region from *cdkn2a*) gene loci in NUP98::HOXA9 ESCs. (A) ImmunoFISH was performed to detect NUP98::HOXA9 nuclear bodies and respective gene loci. The open arrow indicates a co-localized locus. Scale bars, 5 μm.

(B) The minimum distance between each gene locus (as revealed by FISH) and the closest NUP98::HOXA9 nuclear bodies were analyzed using ImageJ (n = 541 for *Hoxa*, n = 274 for Outside).

(C) Schematic representation of NUP98::HOXA9, FG mutant (AG), homeodomain mutant (N51S), or GLFG mutant (GAFG). Yellow bars, asterisk, or blue bars indicate the mutated amino acid residues in the respective construct.

(legend continued on next page)

bodies, their number was significantly reduced. In contrast, the N51S mutation did not inhibit nuclear body formation. However, these were fewer and larger than those formed by the wild-type NUP98::HOXA9 (Figure 3D), consistent with previous studies.[23,62]

Next, we examined the activation of target genes of NUP98::HOXA9 (Figure 3E). This analysis revealed that not only *Hox* cluster genes but other targets of NUP98::HOXA9 in transformed leukemia cells, *Meis1* and *Pbx3*,[15,63] were also activated in NUP98::HOXA9-expressing cell lines. These findings suggest that the mechanism of NUP98::HOXA9-mediated gene activation is highly conserved between mESCs and transformed leukemia cells. Our qPCR results further demonstrate that the formation of nuclear bodies, either by FG or GLFG repeats, is important for the robust activation of *Hox* genes (Figure 3E). Moreover, the ability to form nuclear bodies was reflected in the activation of target genes (wild-type > GAFG > AG).

Furthermore, our ChIP-seq results showed that the accumulation on *Hox* cluster gene loci was significantly diminished in the AG mutant (Figure 3F), which is consistent with a recent report using a similar mutant construct (FG to SG) expressed in hematopoietic stem and progenitor cells.[23] In addition, the DNA-binding-deficient N51S mutation caused a drastic decrease in the ChIP signal in *Hox* clusters. These phenomena were observed for target genes other than *Hox* clusters, such as *Meis1* or *Pbx3*, in mESCs (Figure 3F).

Collectively, these results demonstrate that both phase separation and DNA binding of NUP98::HOXA9 nuclear bodies, two distinct properties of the fusion that rely on NUP98 and HOXA9, respectively, are important for targeting nuclear bodies to target loci to activate downstream genes.

NUP98::HOXA9 nuclear bodies induce the condensation of CRM1 and MLL1 on its target loci

Using these cell lines, we examined whether nuclear bodies formed by NUP98::HOXA9 were associated with MLL1. Strikingly, immunofluorescence analysis revealed that most of the nuclear bodies formed by FLAG-NUP98::HOXA9 co-localized with MLL1 (Figure 4A). We also noticed that these unusual staining patterns of MLL (obvious speckle formation) were only observed in NUP98::HOXA9-expressing ESCs, but not in parental ESCs, AG mutant, or N51S homeodomain-mutant-expressing ESCs. Notably, even if robust NUP98::HOXA9 nuclear bodies were formed in N51S-mutant-expressing cells, MLL1 was not recruited to these nuclear bodies. Therefore, our results suggest that both phase separation (via FG repeats) and proper targeting to specific genomic loci (via a functional homeodomain) are necessary for the formation of NUP98 nuclear bodies that could induce the accumulation of MLL1. These results show that nuclear bodies formed by NUP98::HOXA9 induce the molecular condensation of MLL1, which may increase the local concentration of MLL on *Hox* clusters or other target loci.

To further investigate the role of NUP98::HOXA9 in the accumulation of MLL1 at the target sites, we performed a ChIP-seq analysis (Figures 4B–4E). We found that MLL1 (both MLL1N and MLL1C) is weakly bound to the *Hox* cluster and other target regions in parental ESCs. However, MLL1 robustly accumulates at target sites in a cell line expressing FLAG-NUP98::HOXA9. As for CRM1, we previously demonstrated that ChIP-seq peaks of CRM1 were significantly enhanced in FLAG-NUP98::HOXA9-expressing cells compared with parental ESCs using a polyclonal anti-CRM1 antibody (Bethyl Labs).[33] Here, we noticed that ChIP-seq using a monoclonal anti-CRM1 antibody (CST) showed marked differences in CRM1 ChIP signals between parental ESCs and FLAG-NUP98::HOXA9-expressing cells (Figures 4B–4E).

In addition, we performed ChIP-qPCR and found that these effects were only observed in the *Hox* cluster region in wild-type NUP98::HOXA9-expressing cells, not in AG or N51S mutants (Figure 4F). Moreover, the correlation plot showed strong positive correlations between the binding sites of CRM1 and MLL1 in the parental ESCs, which were significantly enhanced by the expression of FLAG-NUP98::HOXA9 (Figure 4G).

Together, these results show that NUP-fusion proteins are capable of forming molecular condensates with CRM1 and MLL1, which are dependent on phase separation and DNA binding, to induce and/or maintain the activation of a wide range of its targets (Figure 4H).

NUP98::HOXA9 binds both TSS and gene body of *Hox* cluster genes

To elucidate the detailed binding properties of NUP98::HOXA9 and its relevance to gene activation, we performed gene expression profiling and metagenic analysis. Our RNA sequencing (RNA-seq) data showed that 953 genes, including *Hoxa*, *Hoxb*, *Pbx3*, and *Meis1*, were upregulated (upDEGs) in NUP98::HOXA9-expressing ESCs, whereas 445 genes were downregulated (downDEGs) (Figures 5A and 5B). Based on subsequent metagene analysis, although the majority of upDEGs showed an accumulation of NUP98::HOXA9 at the TSS (which we defined as cluster 2 by k-means clustering), in a subset of genes (which we defined as cluster 1), NUP98::HOXA9 showed distinct properties; that is, they bind both the TSS and gene body (Figure 5C). We also confirmed that there was no clear correlation between NUP98::HOXA9 binding and downDEGs or non-differentially expressed genes (nonDEGs) (Figures S3A and S3B). Interestingly, most cluster 1 genes and the upper part of cluster 2, which showed cluster 1-like binding properties (both TSS and gene body), were *Hox* genes (Figure 5C). These results suggest that NUP98::HOXA9, by binding to both the TSS and the gene body simultaneously,

(D) (Left) Confocal imaging of mESCs expressing FLAG-NUP98::HOXA9 or indicated mutants. DAPI staining was used to visualize the nuclei. Enlarged view is shown in the right column. (Right) Protein expression of FLAG-NUP98::HOXA9 and its mutants. GAPDH was used as a loading control.
(E) qPCR analysis of NUP98::HOXA9-target genes (*Hoxa9*, *Hoxa10*, *Hoxb4*, *Hoxb8*, *Meis1*, *Pbx3*) in indicated stable cell lines. Two independent cell lines for each (control, wild-type NUP98::HOXA9, AG mutant, N51S homeodomain mutant, and GAFG mutant) were analyzed. *Gapdh* was used as a reference gene.
(F) Binding profiles of FLAG-NUP98::HOXA9, AG mutant, or N51S mutant in mESC stable cell lines.

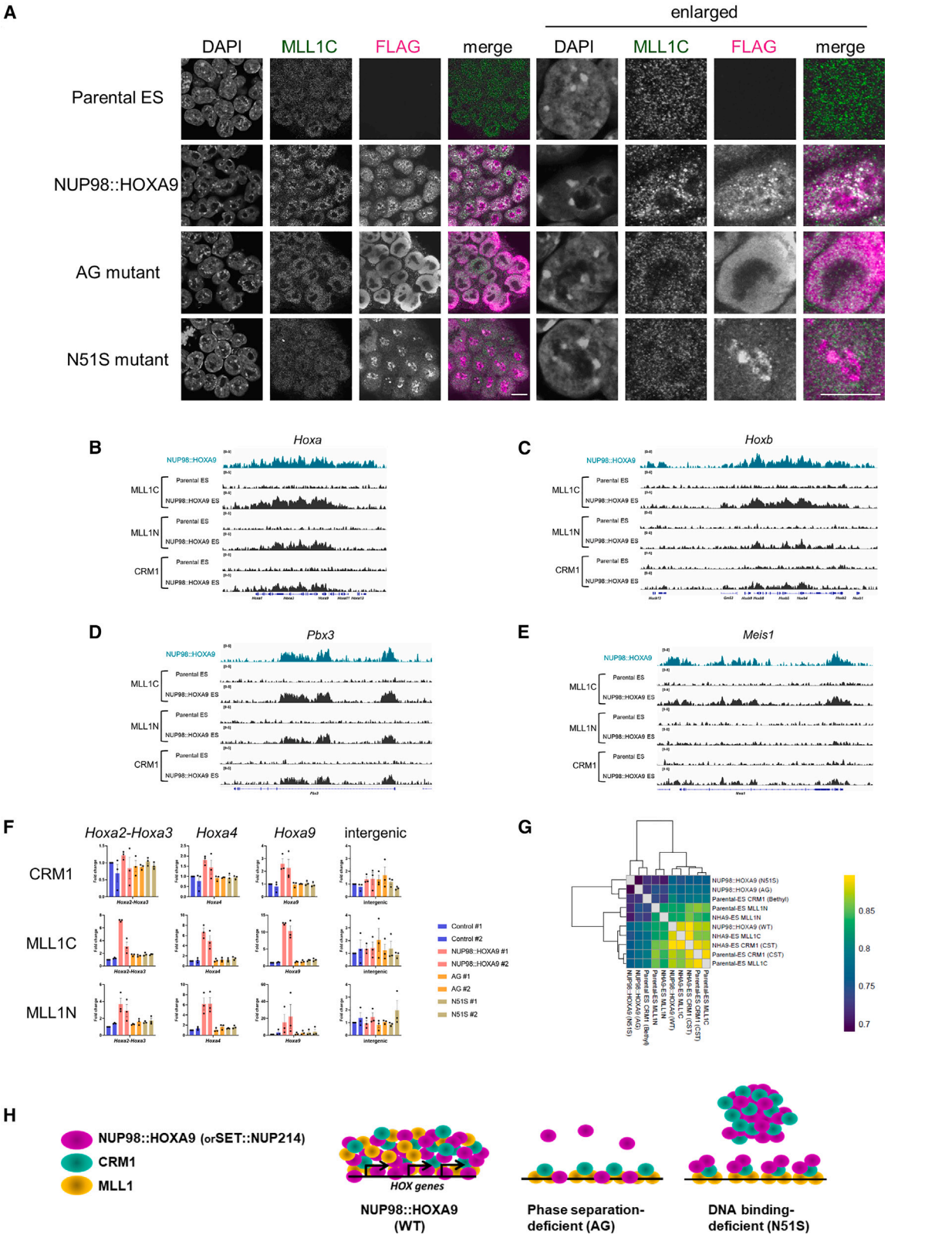

(legend on next page)

could activate its target genes in an unusual manner, which may involve the alteration of the 3D genome structure, as described below.

NUP98::HOXA9 nuclear bodies induce the chromatin loop formation and robust rearrangement of intra- and inter-TAD at its target regions

Recently, NUP98::HOXA9 has been shown to induce chromatin loop formation in HEK293FT cells.[23] Since the mESCs expressing NUP98::HOXA9 used in this study exhibited a more similar gene expression profile of the target genes found in leukemia (for example, *HOXA* genes), we performed Hi-C analysis to compare the effect on high-order chromatin structures. Indeed, we observed an increase in chromatin loops in NUP98::HOXA9-expressing ESCs (~3,500 loops), which was not observed in parental ESCs or phase-separation-deficient AG-mutant-expressing cells (Figure 6A and Table S2). Additionally, the formation of new loops was highly correlated between independent clones (Figure S4). Thus, NUP98::HOXA9 appears to be capable of generating novel chromatin loops, which is consistent with a previous report.[23] However, unexpectedly, NUP98::HOXA9 provoked the rearrangement of topologically associating domains (TADs) in the *Hox* cluster regions, *Pbx3* and *Meis1* loci (Figures 6 and S5). Interestingly, *Hox* regions are located at the boundary between two TADs.[64] *Hox* clusters can interact with and/or be integrated into one of two TADs with distinct properties at a developmental stage or in a tissue-specific manner, which supposedly determines the activity of *Hox* genes.[65–67] We found that NUP98::HOXA9 generated novel chromatin loops, including those between the *HoxA* cluster and *Skap2* (Figures 6A and 6B, closed arrows). Furthermore, we observed alterations in *HoxA*-TAD interactions that coincided with the extension of the boundary region between the two TADs adjacent to the *HoxA* cluster (Figures 6B and S5). Such a drastic effect on the *HoxA* cluster region has not yet been reported in 293FT cells expressing NUP98::HOXA9.[23] We also detected chromatin loops in the *HoxB* cluster region. Notably, we found abrogation of local contacts within *Hox* clusters, particularly *HoxA* and *HoxB*, in NUP98::HOXA9-expressing mESCs, which are most likely compacted domains observed in undifferentiated mESCs (Figures 6A and 6B, open arrows).[68] However, these alterations were less evident in the *HoxC* or *HoxD* clusters (Figure S6).

Surprisingly, NUP98::HOXA9 binding caused severe restriction of the interaction within pre-existing TAD in *Pbx3* and *Meis1* loci (Figures 6B and S5). Notably, these regions, in which drastic changes occur in the 3D genome structure (*HoxA*, *HoxB*, *Pbx3*, *Meis1*), are not often associated with H3K27Ac, a marker of active enhancers,[69] in parental mESCs (Figure S7). Therefore, these results suggest that NUP98::HOXA9 may not utilize pre-existing enhancers, but may rather be capable of generating novel enhancers around its binding sites via the condensation of selected proteins and rearrangement of the 3D genome structure through phase separation.

DISCUSSION

This study demonstrated that the phase separation of NUP fusions can drive the formation of nuclear bodies containing CRM1 and MLL1, which induces the condensation of MLL1 on its binding sites. Moreover, we found that NUP98::HOXA9 altered the high-order genome structure, causing the rearrangement of TADs. Since these activities were not observed in the phase-separation-deficient mutant, our results strongly suggest that phase-separated nuclear bodies of NUP fusion may play two distinct roles: (1) concentration of specific factors for efficient transcription and (2) rearrangement of the 3D genome structure (Figure 7).

Our findings suggest that NUP fusions and MLL1 not only interact with each other but are also essential constituents of molecular condensates (i.e., nuclear bodies) that are presumably suitable for the simultaneous activation of several *HOX* genes that span tens of kilobases apart, as observed in leukemia cells. Consistent with this, MLL1 has been implicated in NUP-fusion activity. NUP98::HOXA9 is directly or indirectly associated with MLL1 and is required for its recruitment to target sites, including *HOX* clusters and downstream gene activation.[14,15] Moreover, MLL1 knockout prevents NUP98::HOXA9-driven leukemogenesis.[14,15] Additionally, SET::NUP214 has been demonstrated to be associated with MLL1 and cooperatively enhances the transcription of *HOXA10*.[22]

MLL1, a histone methyltransferase, and its associated molecules, such as menin, are most likely the primary molecules involved in creating this molecular environment for gene activation. Notably, MLL1 has been linked to RNAPII activity.[70–72] Indeed, we have previously observed enhanced binding of active RNAPII to NUP98::HOXA9 or SET::NUP214 binding sites.[33,43] Therefore, although we cannot fully exclude the possibility that

Figure 4. NUP98::HOXA9 nuclear bodies stimulate the condensation of MLL1 and its accumulation on target sites

(A) Subcellular localization of MLL1C in stable mESCs. Parental mESCs or its stable cell lines expressing FLAG-NUP98::HOXA9, AG mutant, and homeodomain N51S mutant were co-immunostained with anti-MLL1C and FLAG antibodies. DAPI staining for nuclei.

(B–E) Binding profiles of MLL1C, MLL1N, and CRM1 in parental mESC or stable cell lines expressing FLAG-NUP98::HOXA9 as revealed with ChIP-seq (B, *Hoxa*; C, *Hoxb*; D, *Pbx3*; E, *Meis1*).

(F) ChIP-qPCR analysis of CRM1, MLL1C, and MLL1N at *Hoxa* cluster (*Hoxa2-a3*, *Hoxa4*, and *Hoxa9*) and intergenic control region (chr18) in mESCs stably expressing FLAG-NUP98::HOXA9, AG mutant, or N51S homeodomain mutant. Two independent cell lines were used. Data are presented as mean values ± SEM of three independent experiments (n = 3).

(G) Correlation plots of MLL1N, MLL1C, and CRM1 binding sites in parental mESCs (Parental-ES) or NUP98::HOXA9-expressing mESCs (NHA9-ES), together with FLAG-NUP98::HOXA9 (WT, AG, or N51S).

(H) NUP98::HOXA9 or SET::NUP214 forms molecular condensates with CRM1 and MLL1 on its target sites including *HOX* cluster regions. The accumulation of NUP fusion, CRM1, and MLL1 is not observed in phase-separation-deficient mutants. In DNA-binding-deficient mutants, NUP fusion can form nuclear bodies, but these are not substantially associated with the chromatin of target genes. Note that MLL1 is not recruited in these nuclear bodies.

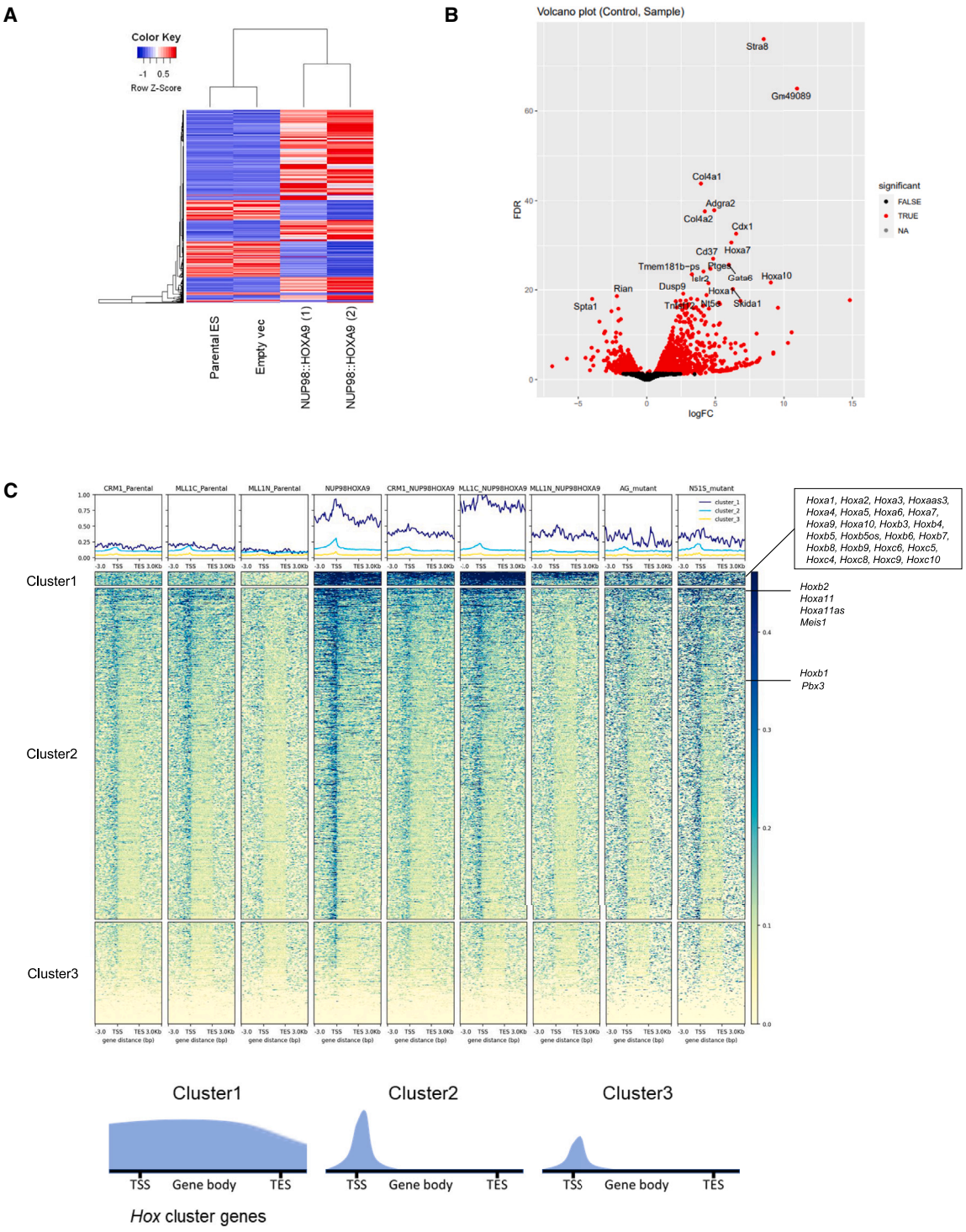

Figure 5. NUP98::HOXA9 binds both TSS and gene body of *Hox* cluster genes

(A) Heatmap of differentially expressed genes (DEGs) in control (parental and empty vector) and NUP98::HOXA9 expressing mESCs (two cell lines).

(B) Volcano plot of gene expression level. Red dots indicate DEGs identified by DESeq2 (false discovery rate [FDR] < 0.05). Selected genes are labeled.

(C) Metagene analysis of indicated proteins. k-means clustering was performed on upregulated DEGs.

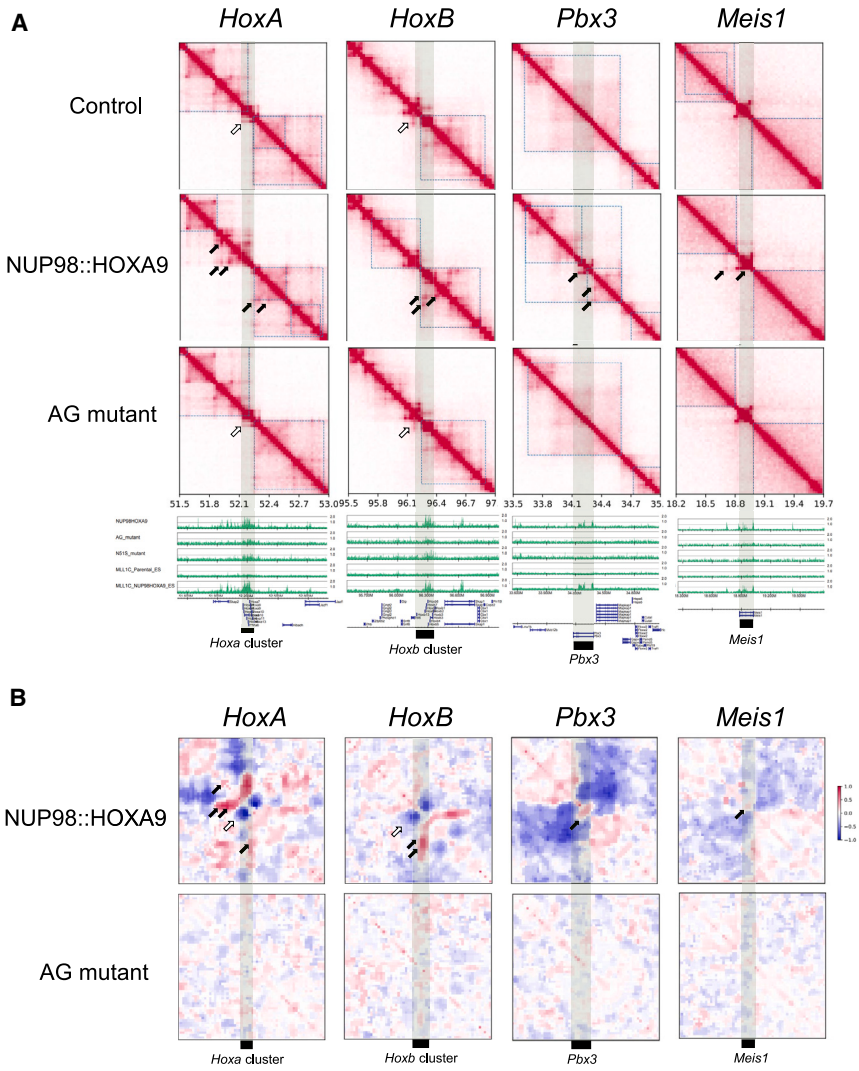

Figure 6. NUP98::HOXA9 nuclear bodies induce the chromatin loop formation and robust rearrangement of intra- and inter-TAD at its target regions

(A) HiC heatmap for *HoxA*, *HoxB*, *Pbx3*, and *Meis1* regions (*HoxA*.chr6.51,500,000–53,000,000; *HoxB*.chr11.95,500,000–97,000,000; *Pbx3*.chr2.33,500,000–35,000,000; *Meis1*.chr11.18,200,000–19,700,000). Specific loops or contacts formed in NUP98::HOXA9-expressing cells are marked with closed arrows, and those lost are marked with open arrows.

(B) Relative enrichment of the interaction frequency (log scale) relative to control.

other unknown factors may also be involved, these appear to be the primary molecules responsible for robust gene activation via phase separation.

Our study further demonstrates that these NUP bodies are maintained in a CRM1-dependent manner. Because CRM1 can even penetrate the FG hydrogel with its cargo,[25] we speculated that NUP98FG or NUP214FG could efficiently hold CRM1 and its associated molecules (possibly MLL1) in the same condensates. However, the mechanism by which CRM1 associates with MLL1 and whether MLL1 contains a functional NES remains unclear.

MLL encodes a large protein that is proteolytically cleaved into the following two fragments: MLL-N and MLL-C.[73,74] MLL1 is predicted to contain significant intrinsically disordered regions (IDRs)[75] and has been reported to form nuclear speckles[76] in which both MLL-N and MLL-C fragments co-localize.[73] Interestingly, a recent study demonstrated that a subcomplex of MLL1 favors a disassembled state and suggested that a high local concentration within a biomolecular condensate could overcome this barrier to assemble the MLL1 complex.[75] Therefore, we speculated that the local condensation of MLL1 by chromatin-bound NUP fusion could stimulate the formation of a functional MLL1 complex on specific gene loci, which is probably difficult to achieve by endogenous MLL1 or other components of the complex alone. In fact, the binding profiles revealed by ChIP-seq showed that the NUP fusion, together with MLL1 and CRM1, bound to an unusually wide range of target gene loci. Thus, the formation of NUP-fusion nuclear bodies on the chromatin seems suitable for creating a molecular environment for the simultaneous activation of multiple target genes located in the neighborhood, as represented by the *HoxA* cluster genes.

Furthermore, our results demonstrate that NUP98::HOXA9 induces a drastic change in the 3D genome structure of mESCs. This is consistent with a recent study[23] in which the authors observed that DNA loops were specifically formed in NUP98::HOXA9-overexpressed 293FT cells. Additionally, the loops frequently overlapped with H3K27Ac marks, leading the authors to conclude that NUP98::HOXA9 induces chromatin loops between proto-oncogene promoters and enhancers to promote malignant transformations. However, an interactome study using BioID suggested that both wild-type and phase-separation-deficient NUP98::HOXA9 (FG to SG mutant) share most of their interacting proteins, including MLL1. In contrast, our results in mESCs expressing NUP98::HOXA9 demonstrated that NUP98::HOXA9 induced the condensation of MLL1 around its target sites (Figure 5C). Therefore, our findings revealed that NUP98::HOXA9 could not only create chromatin loops but could also recruit subsets of proteins, including histone-modifying enzymes, suggesting that NUP98::HOXA9 may not utilize pre-existing enhancers but rather create novel enhancers at its binding sites. Indeed, the profile of the H3K27Ac enhancer mark in the E14 strain (the parental ESC in this study [EB3] is a derivative of E14) demonstrated no signs of strong enhancer sites around

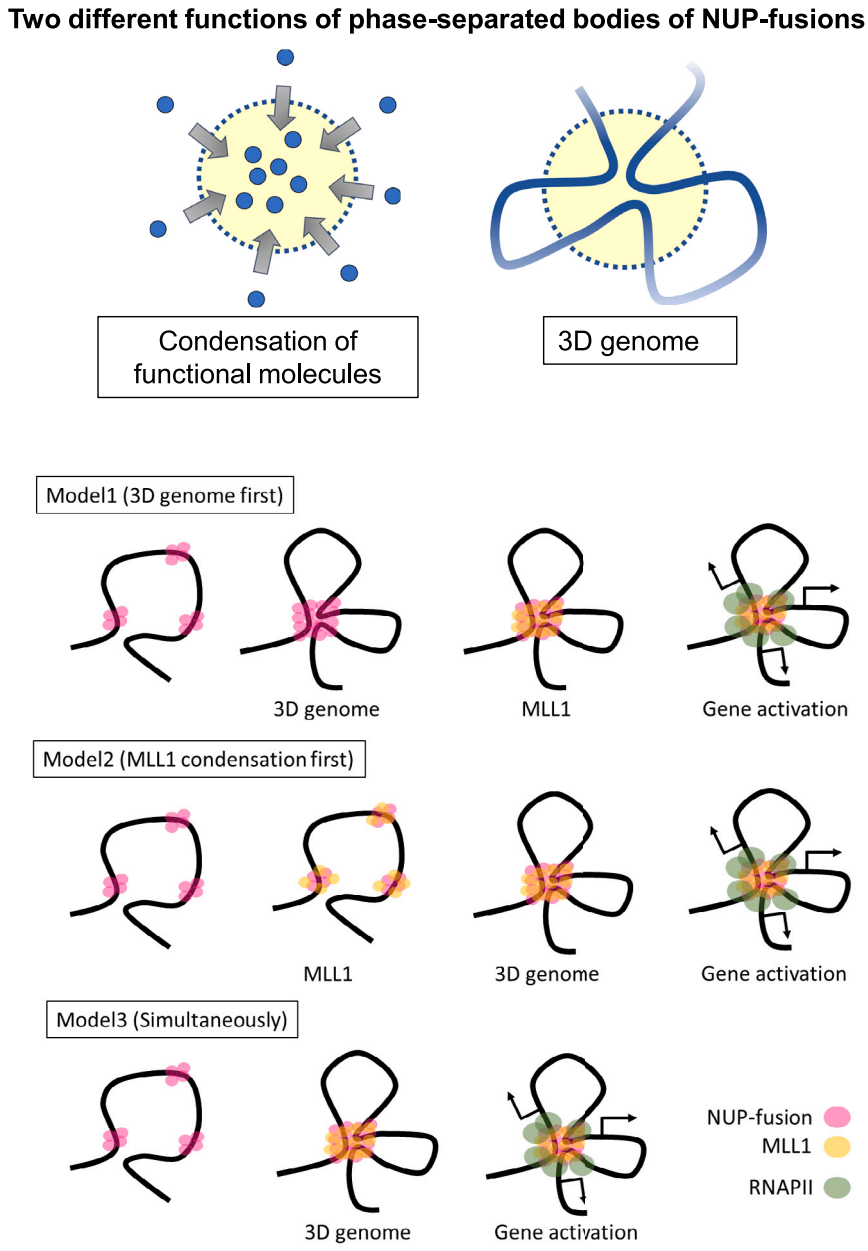

Figure 7. The roles of phase-separated bodies of NUP fusions

A proposed model for the roles of nuclear bodies. The formation of nuclear bodies of NUP fusions causes (1) the condensation of functional molecules, including MLL1, and (2) the alteration of 3D genome structure around its binding regions. These events may finally lead to the recruitment of active RNAP II to induce sustained gene activation. These could be led by 3D genome alteration (model 1), biomolecular condensation (model 2), or simultaneous occurrence (model 3).

the binding sites of NUP98::HOXA9 (*HoxA* and *HoxB* clusters, *Pbx3*, and *Meis1*) (Figure S7). Thus, by increasing the local concentration of MLL1 (and other factors), NUP98::HOXA9 creates a super-enhancer-like environment in which phase separation plays a crucial role.[77–79]

Moreover, NUP98::HOXA9 caused more drastic rearrangements in the 3D genome structure, affecting inter- and intra-TADs. This is interesting because the *Hox* cluster genes *HoxA* and *HoxD* are known to reside at the boundary of two TADs.[64,67,80] Consequently, the modulation of TADs determines the tissue- or developmental-stage-dependent expression pattern of *Hox* cluster genes, called collinearity.[65] Additionally, among the four *Hox* gene clusters (*HoxA*, *B*, *C*, *D*), only *HoxA* and *HoxB*, but not *HoxC* or *HoxD*, showed a robust alteration of the 3D genome structure. This could explain why NUP98::HOXA9 is more prone to activate *HoxA* and *HoxB* cluster genes than *HoxC* and *HoxD* cluster genes.

Collectively, the nuclear bodies formed by NUP98::HOXA9 may be important for both the three-dimensional chromatin architecture and the recruitment and/or concentration of biomolecules such as MLL1 and RNAPII, which are important for the robust activation of the target genes. Future studies are required to elucidate the relationship between molecular condensation, higher-order chromatin structure, and gene activation, all of which are triggered by the nuclear bodies of NUP fusions (Figure 7).

Limitations of the study

Our study demonstrated that the nuclear bodies of NUP-fusion proteins play crucial roles in the condensation of MLL1/CRM1 and the organization of 3D genome structure. However, the data for NUP98::HOXA9 were obtained from stable ESC lines. Although our data showed that the target genes were very similar between leukemia and ESCs, these phenomena need to be examined in more pathophysiologically relevant cells or models.

STAR★METHODS

Detailed methods are provided in the online version of this paper and include the following:

- KEY RESOURCES TABLE
- RESOURCE AVAILABILITY
  - Lead contact
  - Materials availability

SUPPLEMENTAL INFORMATION

Supplemental information can be found online at https://doi.org/10.1016/j.celrep.2023.112884.

ACKNOWLEDGMENTS

We thank Dr. Daisuke Okuzaki for RNA-seq processing, Dr. Koichi Kawakami for transposon vectors, and Dr. Hitoshi Niwa for ESCs. This work was supported by JSPS KAKENHI (20H03444, 17H03679, 16K14676, and 16H06279 [PAGS] to M.O.; 20H00456, 18H05527, 22H04676, and 21H00232 to Y.O.), the Naito Foundation (to M.O.), the Japan Agency for Medical Research and Development (JP22gm6310012h0003 to R.N.), and a BBSRC Impact Acceleration Award (BB/S506783/1) to M.A. This work was partly supported by the Cooperative Research Project Program of the Medical Institute of Bioregulation at Kyushu University.

AUTHOR CONTRIBUTIONS

Conceptualization, M. Oka; methodology, J.A., A.T., M.A., Y.N., K.T., K. Isono, H.K., R.N., and Y.O.; investigation, M. Oka, M. Otani, Y.M., R.O., J.A., T.T., M.A., Y.N., K.T., A.T., K. Ichikawa, S.M., R.N., and Y.O.; supervision, M. Oka, R.N., Y.O., and Y.Y.; writing – original draft, M. Oka; writing – review & editing, M. Oka, M.A., R.N., and Y.Y.

DECLARATION OF INTERESTS

The authors declare no competing interests.

INCLUSION AND DIVERSITY

We support inclusive, diverse, and equitable conduct of research.

Received: January 25, 2023
Revised: May 29, 2023
Accepted: July 13, 2023

REFERENCES

1. Xu, S., and Powers, M.A. (2009). Nuclear pore proteins and cancer. Semin. Cell Dev. Biol. *20*, 620–630. https://doi.org/10.1016/j.semcdb.2009.03.003.
2. Lam, D.H., and Aplan, P.D. (2001). NUP98 gene fusions in hematologic malignancies. Leukemia *15*, 1689–1695.
3. Gough, S.M., Slape, C.I., and Aplan, P.D. (2011). NUP98 gene fusions and hematopoietic malignancies: common themes and new biologic insights. Blood *118*, 6247–6257. https://doi.org/10.1182/blood-2011-07-328880.
4. Michmerhuizen, N.L., Klco, J.M., and Mullighan, C.G. (2020). Mechanistic insights and potential therapeutic approaches for NUP98-rearranged hematologic malignancies. Blood *136*, 2275–2289. https://doi.org/10.1182/blood.2020007093.
5. Zhou, M.H., and Yang, Q.M. (2014). NUP214 fusion genes in acute leukemia (Review). Oncol. Lett. *8*, 959–962. https://doi.org/10.3892/ol.2014.2263.
6. Mendes, A., and Fahrenkrog, B. (2019). NUP214 in Leukemia: It's More than Transport. Cells *8*. https://doi.org/10.3390/cells8010076.
7. Nakamura, T., Largaespada, D.A., Lee, M.P., Johnson, L.A., Ohyashiki, K., Toyama, K., Chen, S.J., Willman, C.L., Chen, I.M., Feinberg, A.P., et al. (1996). Fusion of the nucleoporin gene NUP98 to HOXA9 by the chromosome translocation t(7;11)(p15;p15) in human myeloid leukaemia. Nat. Genet. *12*, 154–158. https://doi.org/10.1038/ng0296-154.
8. Borrow, J., Shearman, A.M., Stanton, V.P., Jr., Becher, R., Collins, T., Williams, A.J., Dubé, I., Katz, F., Kwong, Y.L., Morris, C., et al. (1996). The t(7;11)(p15;p15) translocation in acute myeloid leukaemia fuses the genes for nucleoporin NUP98 and class I homeoprotein HOXA9. Nat. Genet. *12*, 159–167. https://doi.org/10.1038/ng0296-159.
9. Kroon, E., Thorsteinsdottir, U., Mayotte, N., Nakamura, T., and Sauvageau, G. (2001). NUP98-HOXA9 expression in hemopoietic stem cells induces chronic and acute myeloid leukemias in mice. EMBO J. *20*, 350–361. https://doi.org/10.1093/emboj/20.3.350.
10. Kasper, L.H., Brindle, P.K., Schnabel, C.A., Pritchard, C.E., Cleary, M.L., and van Deursen, J.M. (1999). CREB binding protein interacts with nucleoporin-specific FG repeats that activate transcription and mediate NUP98-HOXA9 oncogenicity. Mol. Cell Biol. *19*, 764–776.
11. Bai, X.T., Gu, B.W., Yin, T., Niu, C., Xi, X.D., Zhang, J., Chen, Z., and Chen, S.J. (2006). Trans-repressive effect of NUP98-PMX1 on PMX1-regulated c-FOS gene through recruitment of histone deacetylase 1 by FG repeats. Cancer Res. *66*, 4584–4590. https://doi.org/10.1158/0008-5472.CAN-05-3101.
12. Rio-Machin, A., Gómez-López, G., Muñoz, J., Garcia-Martinez, F., Maiques-Diaz, A., Alvarez, S., Salgado, R.N., Shrestha, M., Torres-Ruiz, R., Haferlach, C., et al. (2017). The molecular pathogenesis of the NUP98-HOXA9 fusion protein in acute myeloid leukemia. Leukemia *31*, 2000–2005. https://doi.org/10.1038/leu.2017.194.
13. Heikamp, E.B., Henrich, J.A., Perner, F., Wong, E.M., Hatton, C., Wen, Y., Barwe, S.P., Gopalakrishnapillai, A., Xu, H., Uckelmann, H.J., et al. (2022). The Menin-MLL1 interaction is a molecular dependency in NUP98-rearranged AML. Blood *139*, 894–906. https://doi.org/10.1182/blood.2021012806.
14. Shima, Y., Yumoto, M., Katsumoto, T., and Kitabayashi, I. (2017). MLL is essential for NUP98-HOXA9-induced leukemia. Leukemia *31*, 2200–2210. https://doi.org/10.1038/leu.2017.62.
15. Xu, H., Valerio, D.G., Eisold, M.E., Sinha, A., Koche, R.P., Hu, W., Chen, C.W., Chu, S.H., Brien, G.L., Park, C.Y., et al. (2016). NUP98 Fusion Proteins Interact with the NSL and MLL1 Complexes to Drive Leukemogenesis. Cancer Cell *30*, 863–878. https://doi.org/10.1016/j.ccell.2016.10.019.
16. Mendes, A., Juhlen, R., Bousbata, S., and Fahrenkrog, B. (2020). Disclosing the Interactome of Leukemogenic NUP98-HOXA9 and SET-

NUP214 Fusion Proteins Using a Proteomic Approach. Cells *17*. https://doi.org/10.3390/cells9071666.

17. Gavory, G., Baril, C., Laberge, G., Bidla, G., Koonpaew, S., Sonea, T., Sauvageau, G., and Therrien, M. (2021). A genetic screen in Drosophila uncovers the multifaceted properties of the NUP98-HOXA9 oncogene. PLoS Genet. *17*. https://doi.org/10.1371/journal.pgen.1009730.
18. Pascual-Garcia, P., Jeong, J., and Capelson, M. (2014). Nucleoporin Nup98 Associates with Trx/MLL and NSL Histone-Modifying Complexes and Regulates Hox Gene Expression. Cell Rep. *9*, 433–442. https://doi.org/10.1016/j.celrep.2014.09.002.
19. Franks, T.M., McCloskey, A., Shokirev, M.N., Benner, C., Rathore, A., and Hetzer, M.W. (2017). Nup98 recruits the Wdr82-Set1A/COMPASS complex to promoters to regulate H3K4 trimethylation in hematopoietic progenitor cells. Genes Dev. *31*, 2222–2234. https://doi.org/10.1101/gad.306753.117.
20. von Lindern, M., van Baal, S., Wiegant, J., Raap, A., Hagemeijer, A., and Grosveld, G. (1992). Can, a putative oncogene associated with myeloid leukemogenesis, may be activated by fusion of its 3' half to different genes: characterization of the set gene. Mol. Cell Biol. *12*, 3346–3355.
21. Van Vlierberghe, P., van Grotel, M., Tchinda, J., Lee, C., Beverloo, H.B., van der Spek, P.J., Stubbs, A., Cools, J., Nagata, K., Fornerod, M., et al. (2008). The recurrent SET-NUP214 fusion as a new HOXA activation mechanism in pediatric T-cell acute lymphoblastic leukemia. Blood *111*, 4668–4680. https://doi.org/10.1182/blood-2007-09-111872.
22. Cigdem, S., Saito, S., Nishikata, D., Nagata, K., and Okuwaki, M. (2021). SET-NUP214 and MLL cooperatively regulate the promoter activity of the HoxA10 gene. Gene Cell. *26*, 830–837. https://doi.org/10.1111/gtc.12886.
23. Ahn, J.H., Davis, E.S., Daugird, T.A., Zhao, S., Quiroga, I.Y., Uryu, H., Li, J., Storey, A.J., Tsai, Y.H., Keeley, D.P., et al. (2021). Phase separation drives aberrant chromatin looping and cancer development. Nature *595*, 591–595. https://doi.org/10.1038/s41586-021-03662-5.
24. Fornerod, M., Boer, J., van Baal, S., Jaeglé, M., von Lindern, M., Murti, K.G., Davis, D., Bonten, J., Buijs, A., and Grosveld, G. (1995). Relocation of the carboxyterminal part of CAN from the nuclear envelope to the nucleus as a result of leukemia-specific chromosome rearrangements. Oncogene *10*, 1739–1748.
25. Labokha, A.A., Gradmann, S., Frey, S., Hülsmann, B.B., Urlaub, H., Baldus, M., and Görlich, D. (2013). Systematic analysis of barrier-forming FG hydrogels from Xenopus nuclear pore complexes. EMBO J. *32*, 204–218. https://doi.org/10.1038/emboj.2012.302.
26. Terlecki-Zaniewicz, S., Humer, T., Eder, T., Schmoellerl, J., Heyes, E., Manhart, G., Kuchynka, N., Parapatics, K., Liberante, F.G., Müller, A.C., et al. (2021). Biomolecular condensation of NUP98 fusion proteins drives leukemogenic gene expression. Nat. Struct. Mol. Biol. *28*, 190–201. https://doi.org/10.1038/s41594-020-00550-w.
27. Chandra, B., Michmerhuizen, N.L., Shirnekhi, H.K., Tripathi, S., Pioso, B.J., Baggett, D.W., Mitrea, D.M., Iacobucci, I., White, M.R., Chen, J., et al. (2021). Phase Separation mediates NUP98 Fusion Oncoprotein Leukemic Transformation. Cancer Discov. *12*, 1152–1169. https://doi.org/10.1158/2159-8290.CD-21-0674.
28. Saito, S., Miyaji-Yamaguchi, M., and Nagata, K. (2004). Aberrant intracellular localization of SET-CAN fusion protein, associated with a leukemia, disorganizes nuclear export. Int. J. Cancer *111*, 501–507. https://doi.org/10.1002/ijc.20296.
29. Saito, S., Cigdem, S., Okuwaki, M., and Nagata, K. (2016). Leukemia-Associated Nup214 Fusion Proteins Disturb the XPO1-Mediated Nuclear-Cytoplasmic Transport Pathway and Thereby the NF-kappaB Signaling Pathway. Mol. Cell Biol. *36*, 1820–1835. https://doi.org/10.1128/MCB.00158-16.
30. Port, S.A., Mendes, A., Valkova, C., Spillner, C., Fahrenkrog, B., Kaether, C., and Kehlenbach, R.H. (2016). The Oncogenic Fusion Proteins SET-Nup214 and Sequestosome-1 (SQSTM1)-Nup214 Form Dynamic Nuclear Bodies and Differentially Affect Nuclear Protein and Poly(A)+ RNA Export. J. Biol. Chem. *291*, 23068–23083. https://doi.org/10.1074/jbc.M116.735340.
31. Oka, M., Asally, M., Yasuda, Y., Ogawa, Y., Tachibana, T., and Yoneda, Y. (2010). The mobile FG nucleoporin Nup98 is a cofactor for Crm1-dependent protein export. Mol. Biol. Cell *21*, 1885–1896. https://doi.org/10.1091/mbc.E09-12-1041.
32. Takeda, A., Sarma, N.J., Abdul-Nabi, A.M., and Yaseen, N.R. (2010). Inhibition of CRM1-mediated nuclear export of transcription factors by leukemogenic NUP98 fusion proteins. J. Biol. Chem. *285*, 16248–16257. https://doi.org/10.1074/jbc.M109.048785.
33. Oka, M., Mura, S., Yamada, K., Sangel, P., Hirata, S., Maehara, K., Kawakami, K., Tachibana, T., Ohkawa, Y., Kimura, H., and Yoneda, Y. (2016). Chromatin-prebound Crm1 recruits Nup98-HoxA9 fusion to induce aberrant expression of Hox cluster genes. Elife *5*, e09540. https://doi.org/10.7554/eLife.09540.
34. Fornerod, M., Ohno, M., Yoshida, M., and Mattaj, I.W. (1997). CRM1 is an export receptor for leucine-rich nuclear export signals. Cell *90*, 1051–1060.
35. Fukuda, M., Asano, S., Nakamura, T., Adachi, M., Yoshida, M., Yanagida, M., and Nishida, E. (1997). CRM1 is responsible for intracellular transport mediated by the nuclear export signal. Nature *390*, 308–311. https://doi.org/10.1038/36894.
36. Ossareh-Nazari, B., Bachelerie, F., and Dargemont, C. (1997). Evidence for a role of CRM1 in signal-mediated nuclear protein export. Science *278*, 141–144.
37. Stade, K., Ford, C.S., Guthrie, C., and Weis, K. (1997). Exportin 1 (Crm1p) is an essential nuclear export factor. Cell *90*, 1041–1050.
38. Krumlauf, R. (1994). Hox genes in vertebrate development. Cell *78*, 191–201.
39. Argiropoulos, B., and Humphries, R.K. (2007). Hox genes in hematopoiesis and leukemogenesis. Oncogene *26*, 6766–6776. https://doi.org/10.1038/sj.onc.1210760.
40. Alharbi, R.A., Pettengell, R., Pandha, H.S., and Morgan, R. (2013). The role of HOX genes in normal hematopoiesis and acute leukemia. Leukemia *27*, 1000–1008. https://doi.org/10.1038/leu.2012.356.
41. Hollink, I.H.I.M., van den Heuvel-Eibrink, M.M., Arentsen-Peters, S.T.C.J.M., Pratcorona, M., Abbas, S., Kuipers, J.E., van Galen, J.F., Beverloo, H.B., Sonneveld, E., Kaspers, G.J.J.L., et al. (2011). NUP98/NSD1 characterizes a novel poor prognostic group in acute myeloid leukemia with a distinct HOX gene expression pattern. Blood *118*, 3645–3656. https://doi.org/10.1182/blood-2011-04-346643.
42. Grier, D.G., Thompson, A., Kwasniewska, A., McGonigle, G.J., Halliday, H.L., and Lappin, T.R. (2005). The pathophysiology of HOX genes and their role in cancer. J. Pathol. *205*, 154–171. https://doi.org/10.1002/path.1710.
43. Oka, M., Mura, S., Otani, M., Miyamoto, Y., Nogami, J., Maehara, K., Harada, A., Tachibana, T., Yoneda, Y., and Ohkawa, Y. (2019). Chromatin-bound CRM1 recruits SET-Nup214 and NPM1c onto HOX clusters causing aberrant HOX expression in leukemia cells. Elife *8*, e46667. https://doi.org/10.7554/eLife.46667.
44. Gorello, P., La Starza, R., Di Giacomo, D., Messina, M., Puzzolo, M.C., Crescenzi, B., Santoro, A., Chiaretti, S., and Mecucci, C. (2010). SQSTM1-NUP214: a new gene fusion in adult T-cell acute lymphoblastic leukemia. Haematologica *95*, 2161–2163. https://doi.org/10.3324/haematol.2010.029769.
45. Lavau, C.P., Aumann, W.K., Sze, S.G.K., Gupta, V., Ripple, K., Port, S.A., Kehlenbach, R.H., and Wechsler, D.S. (2020). The SQSTM1-NUP214 fusion protein interacts with Crm1, activates Hoxa and Meis1 genes, and drives leukemogenesis in mice. PLoS One *15*, e0232036. https://doi.org/10.1371/journal.pone.0232036.
46. Falini, B., Mecucci, C., Tiacci, E., Alcalay, M., Rosati, R., Pasqualucci, L., La Starza, R., Diverio, D., Colombo, E., Santucci, A., et al. (2005). Cytoplasmic nucleophosmin in acute myelogenous leukemia with a normal

karyotype. N. Engl. J. Med. *352*, 254–266. https://doi.org/10.1056/NEJMoa041974.

47. Schlenk, R.F., Döhner, K., Krauter, J., Fröhling, S., Corbacioglu, A., Bullinger, L., Habdank, M., Späth, D., Morgan, M., Benner, A., et al. (2008). Mutations and treatment outcome in cytogenetically normal acute myeloid leukemia. N. Engl. J. Med. *358*, 1909–1918. https://doi.org/10.1056/NEJMoa074306.

48. Falini, B., Brunetti, L., Sportoletti, P., and Martelli, M.P. (2020). NPM1-mutated acute myeloid leukemia: from bench to bedside. Blood *136*, 1707–1721. https://doi.org/10.1182/blood.2019004226.

49. Brunetti, L., Gundry, M.C., Sorcini, D., Guzman, A.G., Huang, Y.H., Ramabadran, R., Gionfriddo, I., Mezzasoma, F., Milano, F., Nabet, B., et al. (2018). Mutant NPM1 Maintains the Leukemic State through HOX Expression. Cancer Cell *34*, 499–512.e9. https://doi.org/10.1016/j.ccell.2018.08.005.

50. Uckelmann, H.J., Haarer, E.L., Takeda, R., Wong, E.M., Hatton, C., Marinaccio, C., Perner, F., Rajput, M., Antonissen, N.J.C., Wen, Y., et al. (2023). Mutant NPM1 Directly Regulates Oncogenic Transcription in Acute Myeloid Leukemia. Cancer Discov. *13*, 746–765. https://doi.org/10.1158/2159-8290.CD-22-0366.

51. Wang, X.Q.D., Fan, D., Han, Q., Liu, Y., Miao, H., Wang, X., Li, Q., Chen, D., Gore, H., Himadewi, P., et al. (2023). Mutant NPM1 Hijacks Transcriptional Hubs to Maintain Pathogenic Gene Programs in Acute Myeloid Leukemia. Cancer Discov. *13*, 724–745. https://doi.org/10.1158/2159-8290.CD-22-0424.

52. Conway, A.E., Haldeman, J.M., Wechsler, D.S., and Lavau, C.P. (2015). A critical role for CRM1 in regulating HOXA gene transcription in CALM-AF10 leukemias. Leukemia *29*, 423–432. https://doi.org/10.1038/leu.2014.221.

53. Mohammed, H., D'Santos, C., Serandour, A.A., Ali, H.R., Brown, G.D., Atkins, A., Rueda, O.M., Holmes, K.A., Theodorou, V., Robinson, J.L.L., et al. (2013). Endogenous purification reveals GREB1 as a key estrogen receptor regulatory factor. Cell Rep. *3*, 342–349. https://doi.org/10.1016/j.celrep.2013.01.010.

54. Dicks, M.D.J., Betancor, G., Jimenez-Guardeño, J.M., Pessel-Vivares, L., Apolonia, L., Goujon, C., and Malim, M.H. (2018). Multiple components of the nuclear pore complex interact with the amino-terminus of MX2 to facilitate HIV-1 restriction. PLoS Pathog. *14*, e1007408. https://doi.org/10.1371/journal.ppat.1007408.

55. Hwang, J., and Pallas, D.C. (2014). STRIPAK complexes: structure, biological function, and involvement in human diseases. Int. J. Biochem. Cell Biol. *47*, 118–148. https://doi.org/10.1016/j.biocel.2013.11.021.

56. Yokoyama, A., Somervaille, T.C.P., Smith, K.S., Rozenblatt-Rosen, O., Meyerson, M., and Cleary, M.L. (2005). The menin tumor suppressor protein is an essential oncogenic cofactor for MLL-associated leukemogenesis. Cell *123*, 207–218. https://doi.org/10.1016/j.cell.2005.09.025.

57. Matkar, S., Thiel, A., and Hua, X. (2013). Menin: a scaffold protein that controls gene expression and cell signaling. Trends Biochem. Sci. *38*, 394–402. https://doi.org/10.1016/j.tibs.2013.05.005.

58. Tai, Y.T., Landesman, Y., Acharya, C., Calle, Y., Zhong, M.Y., Cea, M., Tannenbaum, D., Cagnetta, A., Reagan, M., Munshi, A.A., et al. (2014). CRM1 inhibition induces tumor cell cytotoxicity and impairs osteoclastogenesis in multiple myeloma: molecular mechanisms and therapeutic implications. Leukemia *28*, 155–165. https://doi.org/10.1038/leu.2013.115.

59. Kudo, N., Wolff, B., Sekimoto, T., Schreiner, E.P., Yoneda, Y., Yanagida, M., Horinouchi, S., and Yoshida, M. (1998). Leptomycin B inhibition of signal-mediated nuclear export by direct binding to CRM1. Exp. Cell Res. *242*, 540–547. https://doi.org/10.1006/excr.1998.4136.

60. Shanmugam, K., Green, N.C., Rambaldi, I., Saragovi, H.U., and Featherstone, M.S. (1999). PBX and MEIS as non-DNA-binding partners in trimeric complexes with HOX proteins. Mol. Cell Biol. *19*, 7577–7588.

61. Najbauer, E.E., Ng, S.C., Griesinger, C., Görlich, D., and Andreas, L.B. (2022). Atomic resolution dynamics of cohesive interactions in phase-separated Nup98 FG domains. Nat. Commun. *13*, 1494. https://doi.org/10.1038/s41467-022-28821-8.

62. Fahrenkrog, B., Martinelli, V., Nilles, N., Fruhmann, G., Chatel, G., Juge, S., Sauder, U., Di Giacomo, D., Mecucci, C., and Schwaller, J. (2016). Expression of Leukemia-Associated Nup98 Fusion Proteins Generates an Aberrant Nuclear Envelope Phenotype. PLoS One *11*, e0152321. https://doi.org/10.1371/journal.pone.0152321.

63. Takeda, A., Goolsby, C., and Yaseen, N.R. (2006). NUP98-HOXA9 induces long-term proliferation and blocks differentiation of primary human CD34+ hematopoietic cells. Cancer Res. *66*, 6628–6637. https://doi.org/10.1158/0008-5472.CAN-06-0458.

64. Dixon, J.R., Selvaraj, S., Yue, F., Kim, A., Li, Y., Shen, Y., Hu, M., Liu, J.S., and Ren, B. (2012). Topological domains in mammalian genomes identified by analysis of chromatin interactions. Nature *485*, 376–380. https://doi.org/10.1038/nature11082.

65. Andrey, G., Montavon, T., Mascrez, B., Gonzalez, F., Noordermeer, D., Leleu, M., Trono, D., Spitz, F., and Duboule, D. (2013). A switch between topological domains underlies HoxD genes collinearity in mouse limbs. Science *340*, 1234167. https://doi.org/10.1126/science.1234167.

66. Noordermeer, D., Leleu, M., Schorderet, P., Joye, E., Chabaud, F., and Duboule, D. (2014). Temporal dynamics and developmental memory of 3D chromatin architecture at Hox gene loci. Elife *3*, e02557. https://doi.org/10.7554/eLife.02557.

67. Berlivet, S., Paquette, D., Dumouchel, A., Langlais, D., Dostie, J., and Kmita, M. (2013). Clustering of tissue-specific sub-TADs accompanies the regulation of HoxA genes in developing limbs. PLoS Genet. *9*, e1004018. https://doi.org/10.1371/journal.pgen.1004018.

68. Kundu, S., Ji, F., Sunwoo, H., Jain, G., Lee, J.T., Sadreyev, R.I., Dekker, J., and Kingston, R.E. (2017). Polycomb Repressive Complex 1 Generates Discrete Compacted Domains that Change during Differentiation. Mol. Cell. *65*, 432–446.e5. https://doi.org/10.1016/j.molcel.2017.01.009.

69. Creyghton, M.P., Cheng, A.W., Welstead, G.G., Kooistra, T., Carey, B.W., Steine, E.J., Hanna, J., Lodato, M.A., Frampton, G.M., Sharp, P.A., et al. (2010). Histone H3K27ac separates active from poised enhancers and predicts developmental state. Proc. Natl. Acad. Sci. USA *107*, 21931–21936. https://doi.org/10.1073/pnas.1016071107.

70. Wang, P., Lin, C., Smith, E.R., Guo, H., Sanderson, B.W., Wu, M., Gogol, M., Alexander, T., Seidel, C., Wiedemann, L.M., et al. (2009). Global analysis of H3K4 methylation defines MLL family member targets and points to a role for MLL1-mediated H3K4 methylation in the regulation of transcriptional initiation by RNA polymerase II. Mol. Cell Biol. *29*, 6074–6085. https://doi.org/10.1128/MCB.00924-09.

71. Guenther, M.G., Jenner, R.G., Chevalier, B., Nakamura, T., Croce, C.M., Canaani, E., and Young, R.A. (2005). Global and Hox-specific roles for the MLL1 methyltransferase. Proc. Natl. Acad. Sci. USA *102*, 8603–8608. https://doi.org/10.1073/pnas.0503072102.

72. Milne, T.A., Dou, Y., Martin, M.E., Brock, H.W., Roeder, R.G., and Hess, J.L. (2005). MLL associates specifically with a subset of transcriptionally active target genes. Proc. Natl. Acad. Sci. USA *102*, 14765–14770. https://doi.org/10.1073/pnas.0503630102.

73. Hsieh, J.J.D., Ernst, P., Erdjument-Bromage, H., Tempst, P., and Korsmeyer, S.J. (2003). Proteolytic cleavage of MLL generates a complex of N- and C-terminal fragments that confers protein stability and subnuclear localization. Mol. Cell Biol. *23*, 186–194. https://doi.org/10.1128/MCB.23.1.186-194.2003.

74. Yokoyama, A., Kitabayashi, I., Ayton, P.M., Cleary, M.L., and Ohki, M. (2002). Leukemia proto-oncoprotein MLL is proteolytically processed into 2 fragments with opposite transcriptional properties. Blood *100*, 3710–3718. https://doi.org/10.1182/blood-2002-04-1015.

75. Namitz, K.E.W., Tan, S., and Cosgrove, M.S. (2019). Hierarchical Assembly of the MLL1 Core Complex within a Biomolecular Condensate Regulates H3K4 Methylation. Preprint at bioRxiv, 870667. https://doi.org/10.1101/870667.

76. Yano, T., Nakamura, T., Blechman, J., Sorio, C., Dang, C.V., Geiger, B., and Canaani, E. (1997). Nuclear punctate distribution of ALL-1 is conferred by distinct elements at the N terminus of the protein. Proc. Natl. Acad. Sci. USA *94*, 7286–7291. https://doi.org/10.1073/pnas.94.14.7286.

77. Sabari, B.R., Dall'Agnese, A., Boija, A., Klein, I.A., Coffey, E.L., Shrinivas, K., Abraham, B.J., Hannett, N.M., Zamudio, A.V., Manteiga, J.C., et al. (2018). Coactivator condensation at super-enhancers links phase separation and gene control. Science *361*, eaar3958. https://doi.org/10.1126/science.aar3958.

78. Cho, W.K., Spille, J.H., Hecht, M., Lee, C., Li, C., Grube, V., and Cisse, I.I. (2018). Mediator and RNA polymerase II clusters associate in transcription-dependent condensates. Science *361*, 412–415. https://doi.org/10.1126/science.aar4199.

79. Hnisz, D., Shrinivas, K., Young, R.A., Chakraborty, A.K., and Sharp, P.A. (2017). A Phase Separation Model for Transcriptional Control. Cell *169*, 13–23. https://doi.org/10.1016/j.cell.2017.02.007.

80. Noordermeer, D., Leleu, M., Splinter, E., Rougemont, J., De Laat, W., and Duboule, D. (2011). The dynamic architecture of Hox gene clusters. Science *334*, 222–225. https://doi.org/10.1126/science.1207194.

81. Mu, W., Murcia, N.S., Smith, K.N., Menon, D.U., Yee, D., and Magnuson, T. (2022). RBBP4 dysfunction reshapes the genomic landscape of H3K27 methylation and acetylation and disrupts gene expression. G3 (Bethesda) *12*. https://doi.org/10.1093/g3journal/jkac082.

82. Bi, J., Wang, W., Zhang, M., Zhang, B., Liu, M., Su, G., Chen, F., Chen, B., Shi, T., Zheng, Y., et al. (2022). KLF4 inhibits early neural differentiation of ESCs by coordinating specific 3D chromatin structure. Nucleic Acids Res. *50*, 12235–12250. https://doi.org/10.1093/nar/gkac1118.

83. Wallaert, A., Durinck, K., Van Loocke, W., Van de Walle, I., Matthijssens, F., Volders, P.J., Avila Cobos, F., Rombaut, D., Rondou, P., Mestdagh, P., et al. (2016). Long noncoding RNA signatures define oncogenic subtypes in T-cell acute lymphoblastic leukemia. Leukemia *30*, 1927–1930. https://doi.org/10.1038/leu.2016.82.

84. Durand, N.C., Shamim, M.S., Machol, I., Rao, S.S.P., Huntley, M.H., Lander, E.S., and Aiden, E.L. (2016). Juicer Provides a One-Click System for Analyzing Loop-Resolution Hi-C Experiments. Cell Syst. *3*, 95–98. https://doi.org/10.1016/j.cels.2016.07.002.

85. Dobin, A., Davis, C.A., Schlesinger, F., Drenkow, J., Zaleski, C., Jha, S., Batut, P., Chaisson, M., and Gingeras, T.R. (2013). STAR: ultrafast universal RNA-seq aligner. Bioinformatics *29*, 15–21. https://doi.org/10.1093/bioinformatics/bts635.

86. Love, M.I., Huber, W., and Anders, S. (2014). Moderated estimation of fold change and dispersion for RNA-seq data with DESeq2. Genome Biol. *15*, 550. https://doi.org/10.1186/s13059-014-0550-8.

87. Li, B., and Dewey, C.N. (2011). RSEM: accurate transcript quantification from RNA-Seq data with or without a reference genome. BMC Bioinf. *12*, 323. https://doi.org/10.1186/1471-2105-12-323.

88. Nakato, R.S.T., Wang, J., Nagai, L.A.E., Oba, G.M., Bando, M., and Shirahige, K. (2022). Context-dependent 3D genome regulation by cohesin and related factors. Preprint at bioRxiv. https://doi.org/10.1101/2022.05.24.493188.

89. Langmead, B., and Salzberg, S.L. (2012). Fast gapped-read alignment with Bowtie 2. Nat. Methods *9*, 357–359. https://doi.org/10.1038/nmeth.1923.

90. Zhang, Y., Liu, T., Meyer, C.A., Eeckhoute, J., Johnson, D.S., Bernstein, B.E., Nusbaum, C., Myers, R.M., Brown, M., Li, W., and Liu, X.S. (2008). Model-based analysis of ChIP-Seq (MACS). Genome Biol. *9*, R137. https://doi.org/10.1186/gb-2008-9-9-r137.

91. Li, H., and Durbin, R. (2009). Fast and accurate short read alignment with Burrows-Wheeler transform. Bioinformatics *25*, 1754–1760. https://doi.org/10.1093/bioinformatics/btp324.

92. Isono, K., Endo, T.A., Ku, M., Yamada, D., Suzuki, R., Sharif, J., Ishikura, T., Toyoda, T., Bernstein, B.E., and Koseki, H. (2013). SAM domain polymerization links subnuclear clustering of PRC1 to gene silencing. Dev. Cell *26*, 565–577. https://doi.org/10.1016/j.devcel.2013.08.016.

93. Niwa, H., Masui, S., Chambers, I., Smith, A.G., and Miyazaki, J.i. (2002). Phenotypic complementation establishes requirements for specific POU domain and generic transactivation function of Oct-3/4 in embryonic stem cells. Mol. Cell Biol. *22*, 1526–1536.

94. Ogawa, K., Matsui, H., Ohtsuka, S., and Niwa, H. (2004). A novel mechanism for regulating clonal propagation of mouse ES cells. Gene Cell. *9*, 471–477. https://doi.org/10.1111/j.1356-9597.2004.00736.x.

95. Mohammed, H., Taylor, C., Brown, G.D., Papachristou, E.K., Carroll, J.S., and D'Santos, C.S. (2016). Rapid immunoprecipitation mass spectrometry of endogenous proteins (RIME) for analysis of chromatin complexes. Nat. Protoc. *11*, 316–326. https://doi.org/10.1038/nprot.2016.020.

96. Adachi, J., Hashiguchi, K., Nagano, M., Sato, M., Sato, A., Fukamizu, K., Ishihama, Y., and Tomonaga, T. (2016). Improved Proteome and Phosphoproteome Analysis on a Cation Exchanger by a Combined Acid and Salt Gradient. Anal. Chem. *88*, 7899–7903. https://doi.org/10.1021/acs.analchem.6b01232.

97. Chaumeil, J., Micsinai, M., and Skok, J.A. (2013). Combined immunofluorescence and DNA FISH on 3D-preserved interphase nuclei to study changes in 3D nuclear organization. J. Vis. Exp., e50087. https://doi.org/10.3791/50087.

98. Kawakami, K., and Noda, T. (2004). Transposition of the Tol2 element, an Ac-like element from the Japanese medaka fish Oryzias latipes, in mouse embryonic stem cells. Genetics *166*, 895–899.

99. Urasaki, A., Morvan, G., and Kawakami, K. (2006). Functional dissection of the Tol2 transposable element identified the minimal cis-sequence and a highly repetitive sequence in the subterminal region essential for transposition. Genetics *174*, 639–649. https://doi.org/10.1534/genetics.106.060244.

STAR★METHODS

KEY RESOURCES TABLE

REAGENT or RESOURCE	SOURCE	IDENTIFIER
Antibodies		
anti-FLAG (clone M2)	Sigma-Aldrich	Cat# F1804; RRID:AB_262044
anti-CRM1	Cell Signaling Technology	Cat# 46249S; RRID:AB_2799298
anti-CRM1	BD Transduction Laboratories	Cat# 611833; RRID:AB_399313
anti-CRM1	Bethyl Laboratories	Cat# A300-469A; RRID:AB_451004
anti-NUP214	Bethyl Laboratories	Cat# A300-716A; RRID:AB_533409
anti-MLL1 (C-term)	Cell Signaling Technology	Cat# 14197S; RRID:AB_2688010
anti-MLL1 (N-term)	Cell Signaling Technology	Cat# 14689S; RRID:AB_2688009
anti-Menin	Bethyl Laboratories	Cat# A300-105A; RRID:AB_2143306
anti-GAPDH	Medical & Biological Laboratories	Cat# M171-3; RRID:AB_10597731
anti-ADAR1	Santa Cruz Biotechnology	Cat# sc-73408; RRID:AB_2222767
anti-MX2	Santa Cruz Biotechnology	Cat# sc-271527; RRID:AB_10649506
anti-T3JAM	Santa Cruz Biotechnology	Cat# sc-398781; RRID:N/A
anti-Striatin	Santa Cruz Biotechnology	Cat# sc-136084; RRID:AB_2271282
anti-PARP1	Santa Cruz Biotechnology	Cat# sc-53643; RRID:AB_785086
Anti-Cleaved Caspase-3 (Asp175)	Cell Signaling Technology	Cat# 9661; RRID:AB_2341188
Alexa Fluor 488 Donkey anti-Mouse IgG	Thermo Fisher Scientific	Cat# A21202; RRID:AB_141607
Alexa Fluor Plus 488 Donkey anti-Rabbit IgG	Thermo Fisher Scientific	Cat# A-32790; RRID:AB_2762833
Alexa Fluor 594 Donkey anti-Rabbit IgG	Thermo Fisher Scientific	Cat# A-21207; RRID:AB_141637
Alexa Fluor 647 Donkey anti-Mouse IgG	Thermo Fisher Scientific	Cat# A-31571; RRID:AB_162542
Chemicals, peptides, and recombinant proteins		
Leptomycin B	LC Laboratories	Cat# L-6100
KPT-330	Selleckchem	Cat# S7252
Hygromycin B solution	Wako Pure Chemical	Cat# 084-7681
AMpure XP beads	Beckman Coulter	Cat# A63881
RNase A	Nippon Gene	Cat# 312-01931
DAPI	DOJINDO	Cat# D523
Lipofectamine 2000	Thermo Fisher Scientific	Cat# 11668019
DMSO	Wako Pure Chemical	Cat# 045-24511
ProLong™ Gold Antifade Mountant	Thermo Fisher Scientific	Cat# P36934
Micrococcal nuclease	Worthington Biochemical	Cat# LS004797
GeneAce SYBR® qPCR Mix α Low ROX	Nippon Gene	Cat# 316-07693
Dynabeads™ M-280 Sheep Anti-Rabbit IgG	Thermo Fisher Scientific	Cat# 11203D
Dynabeads™ M-280 Sheep Anti-Mouse IgG	Thermo Fisher Scientific	Cat# 11201D
hybridization buffer	Empire Genomics	Cat# 37CJR2 120
Critical commercial assays		
Nucleofector Kit V	Lonza	Cat# VCA-1003
SMARTer® ThruPLEX® DNA-seq 96D Kit	Rubicon Genomics	Cat# R400407
ReliaPrep RNA Miniprep Systems	Promega	Cat# Z6012
MagMAX mirVana Total RNA kit	Thermo Fisher Scientific	Cat# A27828
PrimeScript™ RT reagent Kit	Takara Bio	Cat# RR037A
Arima-HiC Kit	Arima Genomics	P/N: A510008
Cell Counting Kit-8	DOJINDO	Cat# 347-07621
TruSeq DNA PCR-Free Library Prep Kit	Illumina	Cat# 20015963
TruSeq Stranded mRNA Library Prep Kit	Illumina	Cat# 20020594

(*Continued on next page*)

Continued

REAGENT or RESOURCE	SOURCE	IDENTIFIER
Deposited data		
ChIP-seq	This study	GEO:GSE202837
Hi-C	This study	GEO:GSE222006
RNA-seq	This study	GEO:GSE227199
Proteome data (RIME)	This study	jPOSTrepo:JPST002152
ChIP-seq (H3K27Ac in mESC)	Mu et al.[81]	GEO:GSE183292
ChIP-seq (H3K27Ac in mESC)	Biet al.[82]	GEO:GSE213418
ChIP-seq (H3K27Ac in LOUCY cell)	Wallaert et al.[83]	GEO:GSE74311
Experimental models: Cell lines		
LOUCY	DSMZ	Cat# ACC394; RRID:CVCL_1380
mESC (EB3)	Hitoshi Niwa lab	RRID:CVCL_J647
FLAG-NUP98:HOXA9 ES cell lines	This study	N/A
FLAG-NUP98:HOXA9 (AG mutant) ES cell lines	This study	N/A
FLAG-NUP98:HOXA9 (GAFG mutant) ES cell lines	This study	N/A
FLAG-NUP98:HOXA9 (N51S mutant) ES cell lines	This study	N/A
Oligonucleotides		
Primers for qPCR and ChIP-qPCR	This study	Table S3
siRNA TriFECTa® RNAi Kit for human ADAR1	Integrated DNA Technologies	hs.Ri.ADAR.13
siRNA TriFECTa® RNAi Kit for human KMT2A (MLL1)	Integrated DNA Technologies	hs.Ri.KMT2A.13
siRNA TriFECTa® RNAi Kit for human STRIATIN	Integrated DNA Technologies	hs.Ri.STRN.13
siRNA TriFECTa® RNAi Kit for human MX2	Integrated DNA Technologies	hs.Ri.MX2.13
siRNA TriFECTa® RNAi Kit for human TRAF3IP3	Integrated DNA Technologies	hs.Ri.TRAF3IP3.13
Negative Control DsiRNA	Integrated DNA Technologies	Cat# 51-01-14-03
Recombinant DNA		
AG mutant (NUP98 region of NUP98:HOXA9)	This study	Table S3
GAFG mutant (NUP98 region of NUP98:HOXA9)	This study	Table S3
pT2A-CMH-FLAG(x3)-NUP98:HOXA9	This study	N/A
pCAGGS-m2TP	Koichi Kawakami lab	N/A
pT2A-CMH-FLAG(x3)-NUP98:HOXA9(AG mutant)	This study	N/A
pT2A-CMH-FLAG(x3)-NUP98:HOXA9(GAFG) mutant)	This study	N/A
pT2A-CMH-FLAG(x3)-NUP98:HOXA9(N51S) mutant)	This study	N/A
Software and algorithms		
ImageJ	NIH	https://imagej.nih.gov/ij/
Prism (v8.4.3)	GraphPad	https://www.graphpad.com/
Juicer version 1.6	Durand et al.[84]	https://github.com/aidenlab/juicer
Juicer tools version 2.13.07	Durand et al.[84]	https://github.com/aidenlab/Juicebox/releases
STAR v2.7.10a	Dobin et al.[85]	https://github.com/alexdobin/STAR/releases
DESeq2 v1.36.0.	Love et al.[86]	https://bioconductor.org/packages/release/bioc/html/DESeq2.html
RSEM v1.3.3	Li and Dewey[87]	https://github.com/deweylab/RSEM
CustardPy	Nakato et al.[88]	https://hub.docker.com/r/rnakato/custardpy
Bowtie2 (version 2.3.1)	Langmead and Salzberg[89]	https://bowtie-bio.sourceforge.net/bowtie2/index.shtml
MACS2 (version 2.2.7.1)	Zhang et al.[90]	https://libraries.io/pypi/MACS2
BWA version 0.7.17	Li and Durbin[91]	https://github.com/lh3/bwa
Other		
human *HOXB*	Empire Genomics	RPCI-11 29G13
human *RNF2*	Empire Genomics	RPCI-11 44L12

(*Continued on next page*)

Continued

REAGENT or RESOURCE	SOURCE	IDENTIFIER
mouse *Hoxa*	Isono et al.[92]	RP23-39E6
mouse Outside *Cdkn2a*	Isono et al.[92]	WI1-1292G19
Poly-L-lysine coated coverslip	Neuvitro corporation	Cat# H-15-PDL

RESOURCE AVAILABILITY

Lead contact

Further information and requests for resources and reagents should be directed to and will be fulfilled by the lead contact, Masahiro Oka (moka@nibiohn.go.jp).

Materials availability

All unique reagents generated in this study are available from the lead contact with a completed material transfer agreement.

Data and code availability

- All sequencing datasets generated in this study are available from the GEO repository. The proteomic data are available from the jPOST repository. Accession numbers are listed in the key resources table.
- This paper does not report original code.
- Any additional information required to reanalyze the data reported in this paper is available from the lead contact upon request.

EXPERIMENTAL MODEL AND STUDY PARTICIPANT DETAILS

Cell culture

The leukemia cell line LOUCY was cultured in RPMI1640 medium (Sigma) supplemented with 20% fetal bovine serum (FBS) (Sigma). EB3 ESCs,[93,94] NUP98:HOXA9 stable ESC lines, and their derivatives were cultured in DMEM supplemented with 10% FBS, 10 mM MEM non-essential amino acids (Gibco), 100 mM sodium pyruvate (Gibco), 0.1 mM β-mercaptoethanol (Gibco), and LIF on gelatin-coated dishes.[33] All cells were cultured in a humidified incubator with 5% CO2 at 37°C.

METHOD DETAILS

RIME

RIME was performed as described in Mohammed et al.[95] Cells (1.5×10^7 LOUCY cells per condition) were collected and fixed in serum-free RPMI medium supplemented with 1% (v/v) formaldehyde for 8 min at room temperature. After the addition of 0.1 M glycine to quench crosslinking, the cells were washed twice with ice-cold phosphate-buffered saline (PBS) and resuspended in 500 μL of PBS. After removal of the supernatants, the cell pellets were snap-frozen in liquid N_2 and stored at −80°C. The nuclear fraction of the cells was extracted by resuspending the pellet in 10 mL of LB1 buffer (50 mM HEPES-KOH [pH 7.5], 140 mM NaCl, 1 mM EDTA, 10% glycerol, 0.5% Igepal CA-630, and 0.25% Triton X-100) for 10 min at 4°C with rotation. The cells were collected and resuspended in 10 mL of LB2 buffer (10 mM Tris-HCl [pH 8.0], 200 mM NaCl, 1 mM EDTA, and 0.5 mM EGTA) followed by incubation at 4°C for 5 min with rotation. Cells were pelleted, and resuspended in 300 mL of LB3 buffer (10 mM Tris-HCl [pH 8], 100 mM NaCl, 1 mM EDTA, 0.5 mM EGTA, 0.1% Na-deoxycholate, and 0.5% N-lauroylsarcosine), and sonicated in a water bath sonicator (Diagenode Bioruptor; on ice, 30 s on/off cycle for 20 min). After the addition of 30 μL 10% (v/v) Triton X-100, the samples were vortexed and centrifuged at 20,000 × *g* for 10 min to remove cell debris. The supernatant was then added to 100 μL of magnetic beads (Dynal), preincubated with antibody, and immunoprecipitation (IP) was performed at 4°C overnight. The beads were then washed ten times with 1 mL of RIPA buffer before being washed with a freshly prepared 100 mM ammonium hydrogen carbonate (AMBIC) solution. For the second AMBIC wash, the beads were transferred into new tubes. After removing the supernatant, the samples were stored at −80°C.

To prepare the magnetic beads bound to the antibody, 100 μL of magnetic beads (Dynal) were resuspended in 1 mL of PBS w/5 mg/mL BSA (PBS/BSA) and washed four times with a magnetic separator. After resuspension in 500 μL of PBS/BSA, each antibody was added and incubated overnight with rotation. On the following day, the beads were washed five times with PBS/BSA and used for IP.

Bead-bound proteins were digested with 100 ng trypsin (Promega, V5113) overnight at 37°C. After the overnight digest, 100 ng of trypsin was added to each sample and digested for 4 h at 37°C. The digested peptides were acidified with TFA, desalted, and purified using the C18-SCX StageTips.[96] The peptides were dried using SpeedVac and solubilized in 0.1% formic acid/2% acetonitrile.

Liquid chromatography with tandem mass spectrometry (LC-MS/MS) analysis

LC-MS/MS was performed by coupling an UltiMate 3000 Nano LC system (Thermo Fisher Scientific) and HTC-PAL autosampler (CTC Analytics) to a Q Exactive and Q Exactive Plus hybrid quadrupole-Orbitrap mass spectrometer (Thermo Fisher Scientific). The peptides were delivered to an analytical column (75 μm × 30 cm, packed in-house with ReproSil-Pur C18-AQ, 1.9 μm resin, Dr. Maisch, Ammerbuch, Germany) and separated at a flow rate of 280 nL/min using an 85 min gradient from 5% to 30% of solvent B (solvent A, 0.1% FA and 2% acetonitrile; solvent B, 0.1% FA, and 90% acetonitrile). The Q Exactive and Q Exactive Plus instruments were operated in data-dependent mode. Survey full-scan MS spectra (m/z 350–1,800) were acquired using an Orbitrap with 70,000 resolution after the accumulation of ions to a 3×10^6 target value. The dynamic exclusion was set to 20 s. The 12 most intense multiplied charged ions ($z \geq 2$) were sequentially accumulated to a 1×10^5 target value and fragmented in the collision cell by higher energy collisional dissociation (HCD) with a maximum injection time of 120 ms and 35,000 resolution. Typical mass spectrometric conditions were as follows: spray voltage, 2 kV; heated capillary temperature, 250°C; and normalized HCD collision energy, 25%. The MS/MS ion selection threshold was set to 2.5×10^4 counts. A 3.0 Da isolation width was chosen.

Data processing and visualization

Raw MS data were processed using MaxQuant (version 1.6.14.0) supported by the Andromeda search engine. MS/MS spectra were BLASTed against the UniProt human database using the following search parameters: full tryptic specificity, up to two missed cleavage sites, N-terminal protein acetylation, deamidation (NQ), and methionine oxidation as variable modifications. The false discovery rates of the protein groups and peptides were <0.01. Peptides identified from the reverse database or those identified as potential contaminants were not used.

ImmunoFISH

Immuno-FISH was performed as described in Chaumeil et al.[97] LOUCY cells were pelleted, resuspended in a small volume of PBS, and placed on a poly L-lysine-coated coverslip (Neuvitro Corporation, H-15-PDL). Mouse ESCs were grown on gelatin-coated coverslips. After the fixation of cells in 2% paraformaldehyde/1× PBS for 10 min at room temperature, cells were washed three times in PBS, and permeabilized with ice-cold 0.4% Triton X-100 in PBS for 5 min on ice. The cells were then incubated in 100 μL of blocking solution for 30 min at room temperature and incubated with the primary antibody in 100 μL of blocking solution for 1 h at room temperature. After washing the cells in 0.2% BSA/0.1% Tween 20/PBS three times for 5 min each, the cells were incubated with the secondary antibody diluted in 100 μL of blocking solution for 1 h. The cells were washed three times with 0.1% Tween 20/PBS for 5 min each and fixed in 2% paraformaldehyde/PBS for 10 min. After three washes with PBS, cells were incubated with 0.1 μg/μL RNase A (Nippon Gene) in PBS for 1 h at 37°C in a FISH slide processing system (Thermobrite, ABBOTT). Cells were washed with PBS three times and permeabilized in ice-cold 0.7% Triton X-100/0.1 M HCl for 10 min on ice. After three washes with PBS, the cells were incubated in 50% formamide/2× SSC at 75°C for 30 min and hybridized with labeled BAC probes (RPCI-11 29G13 labeled red for human *HOX-B*) (Empire Genomics), RPCI-11 44L12 labeled green for human *RNF2* (Empire Genomics), RP23-39E6 labeled with Cy3 for mouse *Hox-A*, or WI1-1292G19 labeled with Cy3 for mouse Outside-*Cdkn2a*)[92] for overnight at 37°C using FISH slide processing system. The next day, the cells were washed three times in 50% formamide/2× SSC, 5 min each at 37°C, followed by another three washes in 2× SSC (the last wash was performed with 2× SSC containing 4′,6-diamidino-2-phenylindole (DAPI), 5 min each at 37°C. Cells were mounted in ProLong Gold mounting medium (Thermo Fisher Scientific) and observed under an SP8 confocal microscope (Leica). To evaluate the distance between the nuclear bodies of the NUP fusion and each genomic locus, z stack confocal images of nuclear bodies and FISH were projected in 2D using the max z-projection function in ImageJ. Projected images were binarized, and nuclear body particles were registered using the ImageJ Roi Manager. The distances from the gene loci were calculated using the distance map function in ImageJ. The closest distance to the gene loci was calculated by measuring the minimum intensity on the distance map.

Isolation of stable ESC lines

Parental ESCs were transfected with pCAGGS-m2TP, an expression vector for the Tol2 transposase, and pT2A-CMH-FLAG-NUP98:HOXA9 or its mutants[98,99] using Lipofectamine 2000 (Life Technologies). After 2 days, the cells were trypsinized and replated in an ES-LIF medium containing hygromycin B (200 μg/mL). Colonies were picked and the expression of FLAG-NUP98:HOXA9 or its mutants was examined by immunoblotting and immunofluorescence staining. cDNA encoding NUP98:HOXA9 has been described in,[33] whereas DNA encoding the AG and GAFG mutants of NUP98:HOXA9 was synthesized (GenScript) (Table S3), and the homeodomain (N51S) mutant of NUP98:HOXA9 was generated by PCR-based mutagenesis and cloned into pT2A-CMH-FLAGx3.

Immunostaining and confocal microscopy

Human leukemia LOUCY cells were attached to poly L-lysine-coated coverslips (Neuvitro Corporation, H-15-PDL) and fixed in PBS containing 3.7% formaldehyde for 15 min at room temperature. The cells were washed with PBS and permeabilized with 0.5% Triton X-100 in PBS for 5 min at room temperature. After washing with PBS, the cells were incubated with a blocking buffer (3% skim milk in PBS) for 30 min. The cells were incubated with primary antibodies overnight, washed thrice with PBS, and incubated with secondary antibodies for 30 min. The cells were then washed twice with PBS and stained with DAPI in PBS for 15 min at room temperature. The

cells were mounted using ProLong Gold (Thermo Fisher Scientific). Images were acquired using an SP8 confocal microscope (Leica). ESCs were grown on coverslips and fixed in a medium containing 3.7% formaldehyde for 15 min at room temperature. After washing with PBS, the cells were permeabilized with 0.5% Triton X-100 in PBS for 5 min and further incubated with a blocking buffer (3% skim milk in PBS) for 30 min. The cells were incubated with primary antibodies overnight at 4°C. After washing four times with PBS, the cells were incubated with secondary antibodies for 30 min. The cells were washed four times with PBS, stained with DAPI for 15 min at room temperature, and coverslips were mounted using ProLong Gold mounting medium (Thermo Fischer Scientific). Images were acquired using an SP8 confocal microscope (Leica).

ChIP-qPCR and ChIP-seq

Human leukemia LOUCY cells were fixed in a medium containing 0.5% formaldehyde at room temperature for 5 min. Fixed cells were collected by centrifugation at room temperature, washed twice with ice-cold PBS, and resuspended in ChIP buffer (10 mM Tris-HCl pH 8.0, 200 mM kC), 1 mM $CaCl_2$, 0.5% NP40) containing protease inhibitors (2 μg/mL aprotinin, 2 μg/mL leupeptin, and 1 μg/mL pepstatin A). Cells were briefly sonicated (Branson 250D Sonifier, Branson Ultrasonics), and after centrifugation, the supernatants were digested with 1 U/mL micrococcal nuclease (Worthington Biochemical) for 40 min at 37°C. The reaction was stopped with EDTA (final concentration of 10 mM), and the supernatants were incubated with anti-mouse or anti-rabbit IgG magnetic beads (Dynabeads, Life Technologies) pre-incubated with anti-FLAG M2 (Sigma), anti-CRM1 (CST or Bethyl Lab), anti-NUP214 (Bethyl Lab), anti-MLL1C (CST), and anti-MLL1N (CST) for 6 h. The beads were washed twice with each of the following buffers: ChIP buffer, ChIP wash buffer (10 mM Tris-HCl pH 8.0, 500 mM KCl, 1 mM $CaCl_2$, 0.5% NP40), and TE buffer (10 mM Tris-HCl pH 8.0, 1 mM EDTA) and eluted in an elution buffer containing 50 mM Tris-HCl pH 8.0, 10 mM EDTA, and 1% sodium dodecyl sulfate overnight at 65°C. DNA was recovered using AMPure XP beads (Beckman Coulter) and used for ChIP-qPCR analysis or for library preparation for ChIP-seq analysis.

For ESCs, cells grown in dishes were fixed in a medium containing 0.5% formaldehyde at room temperature for 5 min. After one wash with ice-cold PBS, PBS (0.5 mL) was added and the cells were collected using a scraper. After centrifugation, the collected fixed cells were processed as described above for LOUCY cells, except we used 3 U/mL micrococcal nuclease for chromatin fragmentation.

The ChIP library was prepared using the ThruPLEX DNA-seq kit (Takara Bio) following the manufacturer's instructions and sequenced on an Illumina HiSeq1500 or NovaSeq 6000 system. Adaptor and low-quality sequences were removed, and a read length below 20 bp was discarded using Trim Galore (version 0.6.70). Sequence reads were aligned to the reference mouse genome (mm10) and human genome (GRCh38) using Bowtie2 (version 2.3.1). Multi-mapping and duplicate reads were not used for further analysis. ChIP peaks were identified using MACS2 (version 2.2.7.1), with a p value of <0.001.

qPCR

Total RNA was extracted from cells using the MagMAX mirVana Total RNA kit (Thermo Fisher Scientific) using King Fischer Duo (Thermo Fisher Scientific) or ReliaPrep RNA Miniprep Systems (Promega) and used for cDNA synthesis with the PrimeScript RT reagent Kit (Takara Bio). qPCR analysis was performed in a 384-well plate with the QuantStudio 6 Flex Real-Time PCR System (Life Technologies) using GeneAce SYBR qPCR Mix (Nippon Gene). Relative gene expression levels were normalized to *GAPDH* mRNA levels as a control. The primer sequences are listed in Table S3.

Gene knockdown

LOUCY cells (1×10^7 cells) were transfected with 4 μM of each siRNA (TriFECTa RNAi Kit, IDT) or negative control siRNA (Negative Control DsiRNA, IDT) by nucleofection (Lonza) using Reagent V and the X-001 program. Immediately after nucleofection, the cells were plated on a 100 mm dish in RPMI 1640 medium supplemented with 20% FBS for the indicated period and used for immunoblotting and ChIP-qPCR.[43]

RNA-seq and data analysis

RNA was isolated from mESCs using the ReliaPrep RNA Miniprep System (Promega). RNA libraries were prepared using the TruSeq Stranded mRNA Library Prep Kit (Illumina) following the manufacturer's protocol. Sequencing was performed on a HiSeq 2500 platform in the 75-base single-end mode. Illumina RTA 1.18.64 software was used for base calling. The generated reads were mapped to the mouse (GRCm38/mm10) reference genome using STAR v2.7.10a. Transcripts per million (TPM) and Fragments per kilobase of exons per million mapped reads (FPKM) were calculated using RSEM v1.3.3. Differential expression analysis was performed using DESeq2 v1.36.0.

Hi-C

Hi-C libraries were constructed using the Arima-HiC Kit (Arima Genomics, CA, USA) following the manufacturer's instructions for Mammalian Cell Lines (A160134 v01) and Library Preparation (A160137 v00). Briefly, one million cells were collected and crosslinked with a 37% formaldehyde solution. DNA isolated from the cross-linked cells was digested with two restriction enzymes (GATC and GANTC). After incorporating the biotinylated nucleotides into the digested DNA ends, both ends were ligated to the proximal ends. The ligated DNA was mechanically sheared to an average size of 400–500 bp using a Focused-ultrasonicator M220 (Covaris, MA,

USA), and the ligation junctions were enriched with streptavidin magnetic beads. Sequencing libraries were prepared from enriched DNA fragments using the TruSeq DNA PCR-Free Library Prep Kit (Illumina, San Diego, CA, USA) and amplified for four PCR cycles. The concentration and quality of the libraries were evaluated using a Qubit 4 fluorometer (Thermo Fisher Scientific, Waltham, MA, USA), a 2100 Bioanalyzer System (Agilent Technologies), and a 7900HT Fast Real-Time PCR System (Thermo Fisher Scientific). The final libraries were run on an Illumina NovaSeq 6000 sequencer with a 2 × 150 bp read length.

Hi-C data processing

To process the Hi-C data, we used Juicer version 1.6 and Juicer tools version 2.13.07.[84] Sequenced reads were aligned to the reference mouse genome (mm10) using BWA version 0.7.17,[91] 25-kbp resolution contact matrix with SCALE normalization was generated. TADs (25-kbp resolution) and loops (5-kbp, 10-kbp, and 25-kbp resolutions) were called ArrowHead and HiCCUPS, respectively. The log-scale relative contact frequency and insulation score (500-kbp distance) were calculated using CustardPy.[88]

QUANTIFICATION AND STATISTICAL ANALYSIS

Statistical analysis

GraphPad Prism (Version 8.4.3) was used for data analysis and representation. Data are represented as mean with standard error of means (SEM) with individual data points. The significance of the differences between two groups was determined using two-tailed Student's t-test.